

AtlasRAN: Modeling and Performance Evaluation of Open 5G Platforms for Ubiquitous Wireless Networks

Ryan Barker*, Tolunay Seyfi*, Alireza Ebrahimi Dorcheh*, Julia Boone*, Fatemeh Afghah*, Joseph Boccuzzi[§]

*Holcombe Department of Electrical and Computer Engineering, Clemson University, Clemson, SC, USA

Emails: {rcbarke, tseyfi, alireze, jboone, fafghah}@clemson.edu

[§]NVIDIA Corporation, Santa Clara, CA, USA

Email: jboccuzzi@nvidia.com

Abstract

Fifth-generation (5G) cellular systems are increasingly studied as ubiquitous communication and computing infrastructure for connected vehicles, roadside edge platforms, and future unmanned-system verticals. In this setting, researchers often compare results obtained from simulators, host operating system emulators, digital twins, and hardware-in-the-loop testbeds even though these environments do not preserve timing, input/output (I/O), and control-loop behavior in the same way. Thus, results obtained from them are often not directly comparable. Consequently, apparent limits in throughput, latency, scalability, or real-time behavior may arise from the execution harness rather than from the wireless design itself.

This paper presents *AtlasRAN*, a capability-oriented framework for modeling and performance evaluation of 5G Open Radio Access Network (O-RAN) platforms. *AtlasRAN* introduces two reference architectures, a terminology that distinguishes functional compatibility from timing fidelity, and a capability matrix that maps common research questions to suitable environments. The framework is intended for studies in which 5G acts as shared communications infrastructure across heterogeneous mobility and edge-computing domains. *AtlasRAN* uses O-RAN not as a deployment ideology, but as an experimental coordinate system, including Centralized Units (CU)/Distributed Unit (DU) partitioning, fronthaul transport, control exposure, and core-network anchoring, so that timing, buffering, synchronization, and resource-partition assumptions become measurably explicit. Building on this structure, *AtlasRAN* introduces two reference architectures and a capability matrix that map research questions to the evaluation environments that can support them credibly.

We validate *AtlasRAN* through a CU-DU uplink load study on a coherent CPU-GPU edge platform. Across both a CPU-only baseline and a GPU-accelerated low-density parity-check decoding variant, aggregate goodput drops sharply as the number of user devices increases from 1 to 12, while fairness remains near ideal and compute utilization decreases rather than increases. This combination indicates time-scale dilation and online I/O starvation in the emulation harness, not decoder saturation, as the dominant cause of the observed scaling limit. The practical lesson is that timing, memory, and transport semantics must be reported as first-class experimental variables alongside protocol and machine-learning design choices when evaluating ubiquitous 5G infrastructure.

Index Terms

Ubiquitous Networks, Vehicular Networks, O-RAN, AI-RAN, Digital Twins, 5G/6G, Performance Evaluation

I. INTRODUCTION

Fifth-generation (5G) cellular systems are no longer studied only as mobile broadband networks. They are increasingly treated as a *ubiquitous network*: a shared communication substrate that can support connected road vehicles, roadside infrastructure, sensing nodes, and future unmanned-system services over the same programmable wireless fabric. In this paper, *ubiquitous network* means a communications infrastructure that is continuously available across heterogeneous mobility domains and applications, rather than a network designed for a single fixed use case. This framing is especially relevant for vehicular and shared edge deployments, where reliability, low latency, mobility support, and programmability must coexist within a common infrastructure footprint [1], [2].

This shift raises a practical experimental problem. Modern 5G studies are carried out on a wide range of open and researcher-accessible platforms, including discrete-event simulators, host operating system (host-OS) emulators, software-defined radio (SDR) testbeds, software twins, digital twins, and accelerator-backed execution environments. These platforms may expose similar protocol interfaces while differing substantially in their timing behavior, transport path, buffering model, observability, and hardware partitioning. As a result, papers can appear to disagree about “network performance” when they are in fact measuring different execution harnesses. For ubiquitous-network research, where one infrastructure may be expected to support both vehicular workloads and future unmanned-system services, this distinction directly affects whether a result can inform deployment, control design, or real-time resource provisioning [3]–[6].

Open radio access network (O-RAN) disaggregation and artificial-intelligence radio access network (AI-RAN) workflows make this issue more important, not because every ubiquitous-network deployment must adopt a specific O-RAN stack, but because open disaggregation exposes the interfaces where shared infrastructure is actually coordinated. The Open Distributed Unit (O-DU) and Open Centralized Unit (O-CU) partitioning, radio unit (RU) and open fronthaul interface (OFH) transport, RAN Intelligent Controller (RIC) E2 network orchestration, and 5G Core (5GC) anchoring externalize timing, buffering, synchronization, observability, and resource-partition assumptions that monolithic stacks often hide. Thus claims about “network performance” most often inherit hidden assumptions from the execution harness. *AtlasRAN* therefore uses O-RAN as a coordinate

system for deciding whether a claim is about protocol logic, control policy, or the execution harness itself through its explicit timing, transport, observability, and control semantics. AI-RAN extends the same problem by introducing learning-based functions that may be trained offline, validated in twins, and executed near or inside the signal path.

AtlasRAN addresses this gap by recasting platform selection as a modeling and performance-evaluation problem for ubiquitous wireless infrastructure. We organize the open 5G/6G/O-RAN/AI-RAN landscape around two anchor reference architectures: a Central Processing Unit (CPU)-centric execution path representative of host-OS emulation and software-first O-RAN workflows, and an accelerator-aware path representative of AI-RAN, code-realistic twins, and deployment-grade heterogeneous runtimes. On top of these anchors, we define a capability matrix that makes the following properties explicit: protocol depth, fronthaul realism, timing and I/O fidelity, near-transmission-time-interval control exposure, artificial intelligence insertion points, and per-transmission-time-interval observability. The purpose is not to rank platforms globally, but to identify which platforms are valid for which classes of claims.

The paper then grounds this framework in a quantitative case study. We compare baseline OpenAirInterface (OAI) host-OS radio-frequency simulation (RFSim) against Sionna Research Kit (Sionna-RK), which offloads low-density parity-check (LDPC) decoding to a graphics processing unit (GPU) while preserving much of the surrounding execution path. On a shared coherent CPU-GPU edge platform, both stacks show near-ceiling single-user performance but comparable multi-user collapse as the user-equipment (UE) count grows from 1 to 12. Aggregate uplink goodput drops from 114.59 to 16.35 Mb/s in OAI and from 103.34 to 16.15 Mb/s in Sionna-RK, while Jain fairness stays evenly distributed and CPU/GPU utilization decreases with load. This pattern indicates that the limiting factor is not decoder saturation. Instead, it points to time-scale dilation and online I/O starvation in the emulation harness. The broader systems lesson is important for ubiquitous-network evaluation: coherent memory and accelerator offload can reduce compute pressure, but end-to-end scalability can still be bounded by the surrounding transport and timing semantics.

This interpretation is relevant for various practical applications including shared roadside and edge deployments. Prior edge-focused results show that coherent memory and accelerator offload can reclaim CPU headroom and rebalance work toward the GPU, which is valuable when the same infrastructure node must simultaneously support baseband processing, control logic, and higher-layer autonomy services [7]. *AtlasRAN* extends that line of reasoning by asking what happens *after* a major physical-layer bottleneck is reduced: namely, whether the online execution harness still starves the pipeline. Our answer is yes in the studied host-OS emulation regime, and that answer changes how performance results should be interpreted in wireless ubiquitous-network research.

The main contributions of this paper are:

- **A systems-grounded ubiquitous-network motivation.** We motivate why platform choice must be matched to timing fidelity, control exposure, shared edge compute, and observability when 5G is studied as common infrastructure for vehicular and future unmanned-system workloads.
- **A capability-oriented evaluation framework for open 5G/O-RAN/AI-RAN experimentation.** We justify O-RAN as the systems layer where disaggregation, fronthaul, RIC control, and 5GC anchoring make timing and transport assumptions explicit, and we treat platform selection as part of the modeling and performance-evaluation problem rather than as a tooling choice.
- **A timing-aware execution taxonomy and reference architectures.** We define two anchor execution paths and a precise terminology that separates functional compatibility from timing fidelity across simulation, emulation, software twins, digital twins, and cyber-physical twins.
- **A capability matrix for experiment design.** We map representative research questions—including near-real-time control, full-stack protocol studies, artificial-intelligence insertion, accelerator-backed RAN execution, and twin-to-deployment promotion—to the evaluation environments that provide the required observability, transport semantics, and fronthaul realism.
- **A measurement-backed case study of harness-limited scaling.** Through a CU-DU uplink load study, we show that substantially reducing decoder work does not recover multi-user goodput when the host-OS execution harness becomes the dominant bottleneck, revealing time-scale dilation and online I/O starvation rather than PHY saturation.
- **Practical guidance for reporting and interpreting ubiquitous-network results.** We show that timing discipline, transport path, memory coupling, and per-interval observability should be reported alongside conventional KPIs, because these properties can materially change conclusions about scalability and near-real-time behavior.

II. RELATED WORK

Before turning to *AtlasRAN's* reference architectures, it is useful to position the paper relative to four adjacent lines of work. First, open 5G and O-RAN studies increasingly rely on a diverse set of researcher-accessible platforms, spanning discrete-event simulation, host-OS emulation, SDR/hardware-in-the-loop (HIL) testbeds, software twins, digital twins, and accelerator-backed runtimes [3], [4], [8]–[11]. These platforms often expose similar interfaces while preserving timing, transport, and observability in very different ways, which makes cross-paper comparisons difficult when the execution regime is not made explicit.

Second, recent work on digital twins and automated O-RAN control shows that interface compatibility alone is not enough for defensible performance claims. Twi-Net emphasizes live bidirectional coupling and measurable timing semantics in network twins, while AutoRAN shows that timing, transport, and systems plumbing become first-order variables once open RAN components are scaled and automated under load [5], [6]. These studies sharpen the distinction between functional correctness and time-faithful execution, but they do not provide a unified experiment-design framework spanning the broader open 5G ecosystem.

Third, AI-RAN workflows extend the platform space further by introducing offline differentiable tools, code-realistic twins, and deployment-grade accelerator pipelines [12]–[16]. Adjacent edge-intelligence studies also examine reinforcement-learning-based task offloading and joint communication/computation resource allocation in simulated 5G/O-RAN MEC settings, including

slice-aware PPO/DQN formulations for URLLC and mMTC users [17]. This progression is valuable for future vehicular and unmanned-system infrastructure studies because it connects model development to real-time execution, but it also creates new opportunities to confuse kernel-level speedups with end-to-end system scalability.

Fourth, the emerging AI-RAN Alliance has helped stabilize the terminology around this space by distinguishing *AI-for-RAN*, *AI-and-RAN*, and *AI-on-RAN* [18], [19]. This distinction is useful here because the three categories correspond to meaningfully different experimental intents: improving RAN operation with AI, co-locating AI and RAN workloads on shared infrastructure, and executing AI workloads at the network edge over RAN-resident resources. However, that architectural framing does not by itself tell a researcher whether a specific claim requires offline simulation, host-OS emulation, a code-realistic twin, or a fronthaul-faithful deployment stack. *AtlasRAN* complements the Alliance terminology by mapping those intents to execution regimes with explicit timing, I/O, and observability assumptions.

AtlasRAN addresses the missing layer across these literatures. Rather than reviewing one platform family or one application vertical in isolation, we organize open 5G/O-RAN/AI-RAN environments around execution regime, timing fidelity, fronthaul realism, control exposure, and observability. The goal is to help researchers select an experimental substrate that matches the claim being made, especially when 5G is studied as shared communication and computing infrastructure for vehicular and future unmanned-system workloads. A recurring gap across these literatures is that “open 5G” is often treated as a single category even though host-OS virtual radios, Split 8 SDR deployments, and WG4 7.2x open-fronthaul systems preserve materially different timing and transport contracts. *AtlasRAN* addresses that gap explicitly.

III. *AtlasRAN* FRAMEWORK FOR OPEN 5G/O-RAN EVALUATION

A. Reference Architectures

Having grounded the problem in related work on open 5G experimentation, we now organize *AtlasRAN* around two anchor reference architectures that capture the dominant execution regimes encountered when 5G is studied as ubiquitous infrastructure. The first is a host-based, CPU-centric execution architecture spanning software-only emulation, Split 8 SDR RF-front-end execution, and WG4 7.2x O-RU/OFH realization (Fig. 1). The second is a heterogeneous accelerator-aware path, which reflects emerging AI-RAN workflows in which offline learning, digital twins, and deployment-grade runtimes must be linked across shared models, shared kernels, or shared observability tools (Fig. 2).

These anchors are not presented as the only valid decompositions. Rather, they provide a common vocabulary for judging whether a platform can support a given performance claim with sufficient timing, I/O, and control-loop fidelity. Throughout, we use the following terminology to reduce ambiguity: a *simulator* is offline and not inherently operational; an *emulator* reuses deployment code paths and interfaces but its timing fidelity may not hold under load; a *software twin* provides interface-compatible endpoints (e.g., RU/UE emulation) without full physical-time guarantees; and a *cyber-physical twin* requires a live bidirectional link with explicit coupling and timing semantics [5].

We classify researcher-accessible O-RAN and AI-RAN platforms by *implementation environment* and by the lowest endpoint that closes the radio loop, rather than by nominal performance. Specifically, we organize the ecosystem into: (a) discrete-event simulation (ns-3 with ns-O-RAN extensions) [4]; (b) host-OS emulation, where RAN components execute as user-space processes exchanging protocol messages or software-mediated baseband samples over queues or sockets (e.g., OAI RFSim and srsRAN ZeroMQ) [3], [20]–[25]; (c) Split 8 SDR-based hardware-in-the-loop (HIL), where the full PHY remains in the host gNB/CU/DU stack and a radio front end exchanges time-domain I/Q with the host (e.g., Colosseum/OpenRAN Gym, X5G, and many OAIC-style OTA deployments) [8]–[10], [26], [27]; (d) O-RU/OFH-based HIL, where an O-DU-low terminates native WG4 7.2x open fronthaul toward a compatible O-RU, exposing synchronization, RU capability matching, and fronthaul transport as first-class variables [11], [28], [29]; (e) software twins and digital twins that provide interface-compatible emulation of radios and propagation environments (e.g., software RU/UE emulation and Omniverse-style twins) [30]; and (f) industrial virtualized RAN (vRAN) and AI-RAN stacks that explicitly partition workloads across CPUs, GPUs, and fixed-function accelerators (e.g., FlexRAN and Aerial ACAR) [15], [16]. This taxonomy, summarized in the capability matrix (Table I), provides a common vocabulary for comparing platforms with respect to protocol depth, control-loop exposure, AI insertion points, hardware partitioning, and *fronthaul realism*, which we define to include not only interface contracts (e.g., 7.2x semantics) but also I/O timing, jitter, buffering, and transport behaviors that govern slot deadlines. The CU–DU case study in Sec. IV–V uses this vocabulary to show how an emulator’s transport/time-scale model can dominate multi-UE KPIs, and we present the resulting OAI–SRK comparison artifacts in our open-source repository.¹

Figure 1 should be read as a common host-based, CPU-centric Open RAN substrate with two distinct lower-endpoint realizations rather than as a single host-OS emulation pipeline. In both panels, the shared portion comprises the 5GC, the O-RAN control plane (SMO, non-RT RIC, near-RT RIC), and the higher host-side RAN functions in the O-CU and associated DU processing. In the upper panel, an O-DU-low instance terminates WG4 7.2x open fronthaul and hosts high-PHY and time-critical MAC functions, while the O-RU implements low-PHY/RF. In the lower panel, the host retains the full PHY and exchanges time-domain I/Q with an SDR RF front end, i.e., Split 8. This distinction is essential because the lower endpoint determines whether OFH/eCPRI transport, synchronization, and RU interoperability are first-class experimental variables or are replaced by a simpler RF-front-end interface [26]–[28].

Within this reference architecture, software-only emulation, Split 8 SDR/HIL, and native 7.2x O-RU/OFH execution should not be treated as interchangeable levels of realism. In *software-only configurations*, the radio endpoint is replaced by a channel or transport abstraction that preserves selected baseband or protocol interfaces while removing physical radios and hard real-time constraints. Canonical examples include *RFSim*, where OAI replaces the RF front end with an internal channel model while executing the same gNB code base used in hardware-backed modes [3], [20], [23], and srsRAN’s *ZeroMQ (ZMQ)* virtual-radio

¹<https://github.com/rcbarke/atlasran>

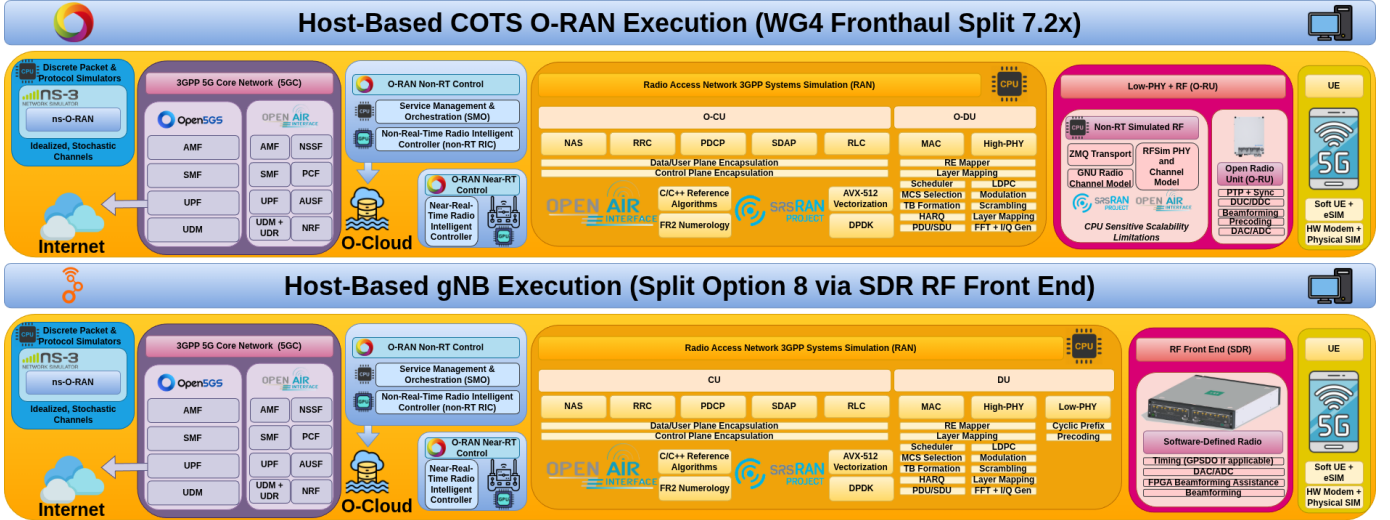


Fig. 1. Host-based CPU-centric 5G execution regimes. **Top:** WG4 fronthaul Split 7.2x, in which an O-DU-low hosted on general-purpose compute implements high-PHY and time-critical MAC functions and exchanges OFH/eCPRI with an O-RU implementing low-PHY/RF; the same panel also highlights software-only RF/channel abstractions used for non-real-time emulation. **Bottom:** Split 8, in which the full PHY remains in the host gNB/CU/DU stack and an SDR acts as the RF front end, potentially with FPGA-based assist functions. The shared 5GC, SMO/RIC, and higher-layer RAN substrate make clear that the main experimental distinction lies in the lower endpoint and thus in which timing, transport, synchronization, and interoperability constraints are actually exposed.

mode, where the stack exchanges baseband I/Q samples between applications over a software transport instead of a physical RF device [24], [25]. In contrast, *Split 8 SDR/HIL* introduces over-the-air impairments and host-to-radio I/Q transport while keeping the full PHY in the host, whereas *native WG4 7.2x* further moves low-PHY/RF into the O-RU and adds OFH/eCPRI transport, PTP/synchronization, and RU capability matching as part of the experiment definition [26], [28], [29]. Both are canonical HIL configurations, but they expose different lower-endpoint contracts: Split 8 SDRs preserve a host-side full PHY and RF-front-end interface, whereas O-RUs add OFH/eCPRI, timing synchronization, and RU capability constraints. Note that in Sec. IV–V, ZMQ is reused as a transport mechanism for a KPM-style monitoring xApp rather than srsRAN’s ZMQ radio mode. We use *software twin* to denote interface-compatible software endpoints that replace hardware devices while preserving external contracts, enabling end-to-end integration testing without physical radios [30].

An *O-DU-low* instance implements high-PHY and time-critical MAC functions at slot granularity, whereas higher-layer DU and CU functions cover the less timing-critical L2/L3 processing. In native WG4 7.2x operation, the *O-RU* implements low-PHY/RF functions and exchanges OFH/eCPRI with the O-DU-low. By contrast, in ordinary Split 8 SDR deployments, the host-side stack retains the full PHY while the *SDR* acts primarily as an RF front end, potentially with FPGA-based digital-front-end assistance (e.g., beamforming weight application or DUC/DDC) without changing the functional split. A *soft UE* denotes a software user-equipment endpoint used for repeatable experimentation without hardware modems. Finally, *per-TTI observability* denotes the ability to instrument and export state at transmission-time-interval granularity (e.g., scheduling decisions, HARQ events, MCS selections, PHY estimates, and AI features). This capability is a key discriminator across O-RAN and AI-RAN platforms, as it determines whether fine-grained near-real-time control loops, reinforcement-learning-based scheduling, high-fidelity dataset capture, and sim-to-real debugging can be supported under O-RAN timing constraints.

Figure 2 illustrates a second reference architecture that underpins emerging AI-native RAN workflows: a heterogeneous “*three computer framework*” spanning offline training, code-realistic digital twins, and real-time GPU-accelerated deployment [16]. In the first stage, offline differentiable simulators are used for large-scale data generation and model training without real-time deadlines (e.g., Sionna and Sionna-RT) [12], [13]. In the second stage, trained components are validated in a code-realistic digital-twin environment that reuses deployment-grade RAN kernels while emulating radios, propagation, and system interactions (e.g., AODT) [16], [30]. In the final stage, selected components are executed in a real-time, GPU-accelerated O-DU connected to software or hardware radio units, where fronthaul I/O and slot-level deadlines must be met (e.g., ACAR) [15], [16]. The key contribution of this architecture is the ability to iteratively transition models across environments, enabling systematic promotion from offline development to deployment-grade execution under realistic timing and I/O constraints.

For the remainder of the paper, we interpret these execution regimes through the needs of ubiquitous-network studies. A vehicular control experiment, a shared-edge observability study, an in-path AI inference study, a Split 8 OTA validation, and a 7.2x fronthaul timing study may all use “5G,” but they do not scope the same experimental substrate. *AtlasRAN*’s taxonomy is intended to prevent those cases from being conflated.

B. Core-Network and Control-Plane Building Blocks for Ubiquitous 5G Experiments

This section corresponds to the *5G core network (5GC)* and *O-RAN Software Community (OSC) control-plane* blocks in Fig. 1. Across the open-source O-RAN ecosystem, these components provide a shared northbound substrate that facilitates a heterogeneous RAN, from simulators and host-OS emulators to SDR/hardware-in-the-loop (HIL) O-DUs and GPU-native stacks, to be configured, monitored, and controlled through common services. In the shared-infrastructure framing adopted here, these components matter because they provide the shared control and anchoring substrate through which heterogeneous mobility

domains can be attached, monitored, sliced, and coordinated over the same 5G infrastructure. While physical layer and medium access control (PHY/MAC) execution environments vary substantially across platforms, reusable control-plane abstractions and 5GC anchoring functions enable end-to-end experiments involving attach procedures, mobility signaling, slicing behavior, and near-real-time closed-loop control.

The OSC control plane operationalizes the O-RAN decomposition through cloud-native implementations of the SMO and the two RAN Intelligent Controller tiers: the non-real-time (non-RT) RIC and the near-real-time (near-RT) RIC. The SMO/non-RT tier operates at coarse time-scales (lifecycle management, KPI aggregation, policy optimization via *rApps*), while the near-RT RIC supports control loops at tens-of-milliseconds to seconds time-scales via *xApps*. In practical open deployments, *xApps* primarily exchange near-real-time telemetry and control with O-CU/O-DU functions over E2 (e.g., E2AP with KPM and RIC Control services), whereas management/configuration is mediated through O1-style interfaces; A1 policy exchange is often partial or realized through custom adapters. Where native E2 agents are absent or incomplete, E2 simulators/emulators (e.g., *e2sim*) can provide a stand-in for integration testing [31]. In Sec. V, our CU-DU case study uses KPM-like L1/L2 KPI monitoring exported over an external ZMQ transport (*xApp*-facing telemetry) to compute resource-level fairness and diagnose scaling artifacts.

Below the RIC/SMO tier, open-source 5GCs provide the control-plane and user-plane anchoring required for end-to-end studies. Two widely used research cores are Open5GS and the OpenAirInterface (OAI) 5GC. Open5GS implements a full 5G SA core and exposes the standard service-based network functions needed for end-to-end experimentation, including AMF, SMF, UPF, AUSF, UDM, UDR, NRF, PCF, NSSF, BSF, and SCP, while also retaining EPC/NSA support for mixed 4G/5G workflows. OAI 5GC likewise spans a broad 3GPP-oriented service-based architecture, with deployment flavors ranging from minimalist configurations centered on AMF, SMF, UPF, and NRF to broader compositions that include UDM, AUSF, UDR, PCF, NSSF, and NEF, together with multiple UPF realizations and containerized or cloud-native deployment options. In practice, the important distinction for *AtlasRAN* is therefore less about missing core functions than about packaging, integration, and experimental surface: Open5GS is often used as a lightweight external research core in O-RAN testbeds, while same-ecosystem deployments may instead pair the RAN with the OAI 5GC or other tightly integrated cores when tighter implementation alignment or richer SBA behavior is desired. Pre-packaged variants of Open5GS, such as *srsRAN*'s dockerized variant, often implement minimalistic AMF, SMF, UPF, and Subscriber Database functions, preserving advanced features such as NSSF, NRF, and PCF for custom deployment configurations. Accordingly, *AtlasRAN* treats 5GC selection as a question of integration surface, observability, control exposure, and deployment complexity rather than as an assumed absence of advanced core capabilities [3], [20], [32].

Across the ecosystem in Fig. 1, the SMO/RIC/5GC tier induces two recurring integration patterns relevant to experimental design. *Integrated end-to-end stacks* couple a 5GC and RAN implementation within a single distribution, enabling rapid end-to-end experimentation with minimal integration overhead. In contrast, *RAN-only* stacks focus on O-DU/O-CU functionality and rely on external 5GCs for mobility management, session control, and user-plane anchoring, which is common when the experimental emphasis is on RAN execution (e.g., PHY/MAC behavior, fronthaul realism, accelerator partitioning, or near-RT control) and enables modular substitution of the core network without altering the RAN implementation.

C. Open-Source RAN Stacks Across Evaluation Regimes

One practical consideration in this context is what execution regime is appropriate when investigating a specific ubiquitous-network claim. We first consider CPU-centric execution regimes, as illustrated in Fig. 1, and consolidate the open-source RAN landscape along a practical progression: discrete-event simulation \rightarrow host-OS emulation \rightarrow SDR/HIL operation. We emphasize platforms that are widely used and researcher-accessible, while making explicit where performance-relevant behaviors are properties of the *execution harness*, including operating-system (OS) scheduling, transport behavior, and timescale preservation, rather than of protocol correctness. This distinction is central to the CU-DU case study presented later, where we quantify how timing- and I/O-sensitive key performance indicators (KPIs) can be dominated by the evaluation environment even when the underlying PHY implementation is unchanged.

a) Discrete-event simulation: ns-3 + ns-O-RAN: ns-O-RAN extends ns-3 with explicit models for O-Cloud resources, near-RT RICs, and the E2 interface, allowing RAN nodes, controllers, and applications to run as C/C++ objects within a single deterministic event-driven simulation [4]. This yields fully repeatable experiments that are unaffected by host OS scheduling noise and can scale to thousands of UEs and cells. ns-O-RAN supports multiple numerologies, bandwidths, and mmWave channels at packet and frame granularity, and can attach abstracted SMO and RIC logic to study slicing and control-plane policies; however this abstraction prices realism: it has no HIL mode, no integration with SDRs or O-RUs, and no 7.2x fronthaul, so policies trained solely in ns-O-RAN must be adapted before running on SDR or HIL platforms that expose different RF impairments and timing. Extending ns-O-RAN to new numerologies or architectures typically requires non-trivial C/C++ model and scenario refactoring [4]. In short, ns-O-RAN offers maximal scalability and determinism but minimal RF fidelity.

b) Eurecom OpenAirInterface: OAI provides a 3GPP-aligned 5G NR implementation with broad Rel-15 and core Rel-16 support spanning the full gNB protocol stack (PHY through L3), and it exposes several distinct execution regimes that should not be conflated: RFSim for software-only emulation, ordinary Split 8 front-end operation, and a separate O-RAN 7.2 CUS-plane path for compatible O-RUs [3], [20], [27]. A key practical advantage is that these regimes share a common code base and configuration philosophy, allowing researchers to develop protocol-layer modifications and instrumentation in software-only settings and then “promote” them to over-the-air or O-RU-backed execution when stronger RF or fronthaul realism is required.

OAI's RFSim mode executes a largely complete NR stack—PHY through 5GC—entirely on the CPU, with RF interactions replaced by an internal channel simulator [3], [20]. Importantly, Eurecom's own RFSimulator documentation makes explicit that RFSim is an *emulation* convenience rather than a timing-faithful RF substitute: “*it works like an RF board, but not in real-time: It can run faster than real-time if there is enough CPU, or slower*” [23]. In other words, RFSim can run faster or

slower than wall-clock time depending on CPU availability and the chosen scenario, and its sample-forwarding transport can introduce backpressure that is external to the logical NR protocol design; thus, timing-sensitive KPIs under multi-UE load can be dominated by the emulation harness rather than the intended baseband bottleneck [5]. We quantify this effect in Sec. V-A, using a controlled CU-DU load-test methodology within Sec. IV-A. Our testing harness is applied consistently across OAI and another hardware-offloaded 5G stack, Sionna Research Kit (SRK).

OAI-SDR corresponds to ordinary Split 8 front-end operation, most commonly with UHD-supported USRPs in open-source research practice, and should not be described as native WG4 7.2x fronthaul. OAI roadmap material explicitly distinguishes UHD/USRP front ends (Split 8) from the separate O-RAN 7.2 CUS-plane path [27]. In this mode, OAI preserves the same full gNB/CU/DU software path used in RFSim while replacing the virtual RF board with physical radio hardware, enabling OTA trials with COTS UEs and exposing practical concerns absent in RFSim: radio-front-end stability, host scheduling, synchronization, and I/Q transport overhead [3], [20], [33]. OAI-SDR therefore underpins RF-facing infrastructures such as Colosseum/OpenRAN Gym, X5G, and OAIC when protocol completeness and OTA repeatability dominate, but it remains a Split 8 regime rather than an open-fronthaul/O-RU one [8]–[10].

OAI-O-RU corresponds to OAI’s distinct open-fronthaul mode, in which the DU terminates the O-RAN 7.2 CUS-plane toward a compatible O-RU rather than a Split 8 radio front end. Current OAI materials describe this path as an O-RAN 7.2 fronthaul integration using the OSC xRAN library, separate from UHD/USRP operation and associated with explicit 7.2-specific build, interoperability, and timing considerations [27], [29]. Relative to OAI-SDR, this mode makes fronthaul transport, RU capability matching, synchronization, and 7.2x interoperability first-class experimental variables, and it is therefore the appropriate OAI regime when the claim depends on native O-RU behavior or open-fronthaul realism rather than merely OTA execution.

In aggregate, OAI prioritizes standards compliance and protocol completeness over aggressive microarchitectural optimization. Its LDPC and Turbo decoders are baseline-compliant but only lightly vectorized, there is no native DPDK-based user-plane offload, and inter-layer communication relies on legacy, copy-heavy data structures inherited from LTE-era RLC implementations. While these design choices simplify correctness and maintainability, they can introduce encapsulation buffer overflows—particularly in the RLC and GTP-U layers—even at modest UE counts. In several OpenRAN Gym deployments, the E2 application protocol (E2AP) is terminated in a separate e2sim-based process, while the gNB hosts only the E2 service-model (E2SM) logic and exchanges E2SM payloads with e2sim over local transports (e.g., UDP), motivating co-location of the gNB and e2sim to limit added latency and jitter [31], [34].

c) *Software Radio Systems RAN*: srsRAN follows a performance-oriented design philosophy that differs from OAI. Its gNB/CU/DU implementation is optimized for efficient CPU execution, with a complete L1/2/3 stack and a configuration surface oriented toward high-throughput FR1 experimentation [21], [35], [36]. In practice, the project exposes three distinct regimes that should be kept separate in *AtlasRAN*: virtual-radio/ZMQ execution for software-mediated end-to-end testing, ordinary Split 8 RF-front-end operation with SDRs, and a separate Split 7.2 path for compatible O-RUs via the Open Fronthaul (OFH) library [26], [28]. Similar to OAI, srsRAN supports both software-only execution and SDR-based over-the-air operation; however, its software-only mode is explicitly positioned as a protocol emulation environment rather than a fully standard-compliant 5G NR physical-layer simulator, prioritizing fast iteration and control-plane experimentation over detailed PHY fidelity.

In its ZeroMQ (ZMQ) mode, srsRAN uses a virtual radio that exchanges baseband I/Q samples between applications over ZeroMQ instead of a physical RF device [24], [25]. This path is documented for development, testing, debugging, CI/CD, teaching, and proof-of-concept end-to-end experiments, and the same tutorials describe both ZMQ-based setups and OTA setups with physical radios [24], [25]. As such, liberties are taken within srsRAN simulations, partially within the low physical layer digital signal processing (DSP) pipeline, and the platform does not claim full 3GPP conformance within this operational mode. When paired with AmariUE, ZMQ mode provides a convenient software-mediated path for exercising the gNB against a commercial UE emulator; when paired with the prototype srsUE path, the documentation explicitly positions the setup as initial testing rather than deployment-ready operation, with current 5G SA limitations including 15 kHz SCS/FDD-only operation, 5–20 MHz bandwidths, and no handover [24], [25]. For *AtlasRAN*, the key implication is that srsRAN-ZMQ is strong for protocol integration, core attach, E2/xApp development, and controlled repeatability, but it is not the right mode for claims that depend on RF impairments, native open-fronthaul transport, or deployment-grade UE realism.

srsRAN-SDR targets high-throughput FR1 operation on COTS servers. It corresponds to ordinary Split 8 RF-front-end operation, not native WG4 7.2x fronthaul. The official CU-DU split tutorial states explicitly that using a USRP as the RF front end results in a Split 8 configuration and directs users to the RU Guide for Split 7.2x deployments [26]. In this mode, srsRAN drives SDR hardware such as the USRP B210 while exposing the practical concerns absent from ZMQ mode: over-the-air impairments, front-end stability, host scheduling, and I/Q transport overhead. srsRAN-SDR supports a broad range of FR1 numerologies, with configuration files intended for multi-cell, multi-UE experiments and rapid iteration [37]. Due to its many optimizations, srsRAN-SDR is a natural choice for stressing schedulers and L2/L3 behavior under load when FR1 suffices and when researchers want a configuration surface tailored to performance-oriented experimentation [21], [26], [37]. Limitations include narrower FR2 support (with $\mu = 3$ 120 kHz SCS still roadmapped) and the absence of a fully open-source, software-only 5G-SA NR PHY.

srsRAN-O-RU/OFH is the separate native Split 7.2 mode. The official RU Guide states that srsRAN supports both Split 7.2 and Split 8 fronthaul interfaces to RUs, and that the Split 7.2 path is implemented through the Open Fronthaul (OFH) Library to interface the CU/DU with third-party O-RUs [28]. Unlike ordinary SDR mode, this path requires explicit fronthaul switching and time-synchronization engineering and makes RU capability matching, OFH transport, and timing topology part of the experiment definition. This is therefore the correct srsRAN regime when the claim depends on native WG4 7.2x behavior or O-RU interoperability rather than merely RF-facing OTA execution [28].

In aggregate, srsRAN prioritizes execution efficiency and experimental throughput in FR1 more aggressively than OAI, particularly in the upper PHY, MAC, and surrounding protocol layers. The project’s architecture and tuning guidance emphasize CPU-efficient DU-high/DU-low partitioning, aggressive low-level optimization for hot-path signal-processing and scheduling

routines, and optional high-performance packet-I/O acceleration through DPDK acceleration and/or gRPC stateless streaming when CU/DU throughput or O-RU traffic stability become limiting factors [21], [26], [28], [35]. In practice, this makes srsRAN especially attractive for studies where the goal is to stress scheduler behavior, protocol scaling, and FR1 load-bearing capacity on COTS compute rather than to maximize standards-completeness across every execution mode. Relative to OAI, the resulting trade-off is a leaner, more performance-oriented software path for high-PHY and protocol-layer experimentation, with cleaner scaling behavior under CPU pressure, while accepting that some software-only and emulator-facing workflows are intentionally positioned for rapid integration and testing rather than for full deployment-grade PHY fidelity [36], [37].

Cross-cutting limitations of CPU-centric stacks. Across ns-O-RAN, host-OS emulation modes (OAI RFSim and srsRAN ZMQ), and SDR-based CPU gNBs, a shared constraint is that key timing behaviors emerge from the interaction of protocol implementations with general-purpose operating systems and user-space transports. Host scheduling jitter, CPU contention, and non-deterministic transport artifacts can invalidate modeling assumptions often implicit in learning-based control (e.g., stationarity and Markovian state evolution), and materially affect sim-to-real transfer when moving from deterministic simulators to real-time pipelines [38]. Even when functional correctness is achieved, CPU ceilings and copy-heavy software paths can limit scaling to larger UE counts or wider bandwidths without dedicated acceleration, motivating the separation between “CPU-centric” experimentation and later-stage HPC or GPU-backed designs captured by Fig. 2; Sec. V makes this concrete by measuring how host-OS emulation timing and transport effects can dominate multi-UE UL scaling even when the PHY decoder is accelerated.

D. Accelerator-Backed RAN Execution and the Shift from Compute Limits to I/O Limits

This section marks the transition from software-first experimentation to heterogeneous acceleration execution (Fig. 2), where the main question becomes how work is partitioned across the CPU, accelerator, and transport path. For ubiquitous 5G infrastructure, this transition is important because edge nodes must often support radio processing together with sensing, control, and higher-layer autonomy workloads. In that setting, accelerator offload is valuable not only when it increases raw throughput, but also when it rebalances scarce compute resources in a predictable way. At the same time, once a major physical-layer bottleneck is reduced, the dominant limit often moves outward to memory movement, host orchestration, and fronthaul-facing I/O.

Within this regime, in the quest to reclaim headroom for RIC-orchestrated AI, Intel FlexRAN serves as an evolutionary bridge between software gNBs and AI-RAN: it retains a CPU-resident control and integration surface while offloading the most compute-intensive PHY primitives to fixed-function acceleration. These accelerators range from PCIe-attached devices (e.g., ACC100-class forward-error-correction offload via DMA) to more tightly integrated, on-CPU acceleration engines (e.g., ACC200 / vRAN Boost on Sapphire Rapids), which reduce data-movement overhead while preserving a similar functional split; accordingly, LDPC/Turbo decoding and FFT-class workloads are delegated to accelerators while higher-layer processing remains CPU-resident [15], [39], [40]. The open stacks encompassed in Section III-C (e.g., OAI and srsRAN) can also be paired with vendor acceleration paths (e.g., NIC/DPDK and FEC offload where supported), but the practical integration surface and end-to-end plumbing often differ from FlexRAN- or CloudRIC-style references, where the acceleration boundary is explicitly engineered as part of the platform architecture [40], [41].

However, the presence of an accelerator does not, by itself, solve end-to-end real-time RAN execution: once compute-heavy kernels are accelerated, the bottleneck often shifts to I/O and memory movement—PCIe transfers, buffer orchestration, and copy-heavy data paths can dominate the critical path and reintroduce timing variance even when the underlying PHY kernels are fast [15], [41]. This is particularly acute in fronthaul-facing pipelines, where slot deadlines couple compute to high-rate packet/sample ingress and egress; as a result, practical scalability depends on system-level plumbing (e.g., minimizing copies, reducing kernel crossings, and stabilizing host scheduling) as much as on raw accelerator throughput. Our CU–DU results in Sec. V-D make this point concrete: decoder offload can reduce cumulative LDPC work, yet multi-UE goodput can remain constrained by transport/timing fidelity in the surrounding execution harness.

Observing UE constriction within emulators motivates the shift in Section III-E toward GPU-native stacks whose contributions are not limited to GPU kernels, but include pipeline-level, low/zero-copy I/O designs (e.g., kernel-bypass networking and direct device-to-accelerator data movement) that reduce memory traffic and jitter in the fronthaul-to-baseband path [16], [42]–[44]. This systems shift is central to the paper’s later argument: coherent memory and offload can reduce decoder work, yet end-to-end scalability may still be set by online I/O starvation in the surrounding evaluation harness.

E. From Differentiable Modeling to Deployment-Grade Runtime for Ubiquitous AI-RAN Studies

For ubiquitous-network research, the main value of AI-RAN toolchains is not simply that they enable machine learning. Their value is that they create a promotion path from offline modeling, to code-realistic twin environments, to deployment-grade runtime systems in which timing and transport constraints become visible. Aligned with Fig. 2, we therefore trace an AI-RAN workflow from differentiable “physics engines” to GPU-native RAN execution and digital twins. The key shift relative to CPU-centric stacks is that capability is determined not only by which NR procedures are implemented, but also by where they execute (CPU versus GPU versus data processing unit, DPU) and how data transports are engineered (model I/O, fronthaul I/O, and observability). This makes these toolchains especially useful when one wants to move from dataset-driven development to claims about online inference, shared edge infrastructure, or slot-level control behavior.

a) *Differentiable physics engines—Sionna PHY/SYS and Sionna-RT:* The Sionna family provides a differentiable physical-layer substrate for *offline* AI-for-RAN workflows, emphasizing batch throughput and end-to-end differentiability rather than slot-deadline execution. Sionna implements 5G-aligned waveforms, coding, propagation abstractions, and neural receiver components (e.g., learned demappers/decoders) in a GPU-accelerated TensorFlow framework, enabling gradient-based modem design and large-scale dataset generation [12]. Sionna is organized around *Sionna PHY* (link-level simulation) and *Sionna*

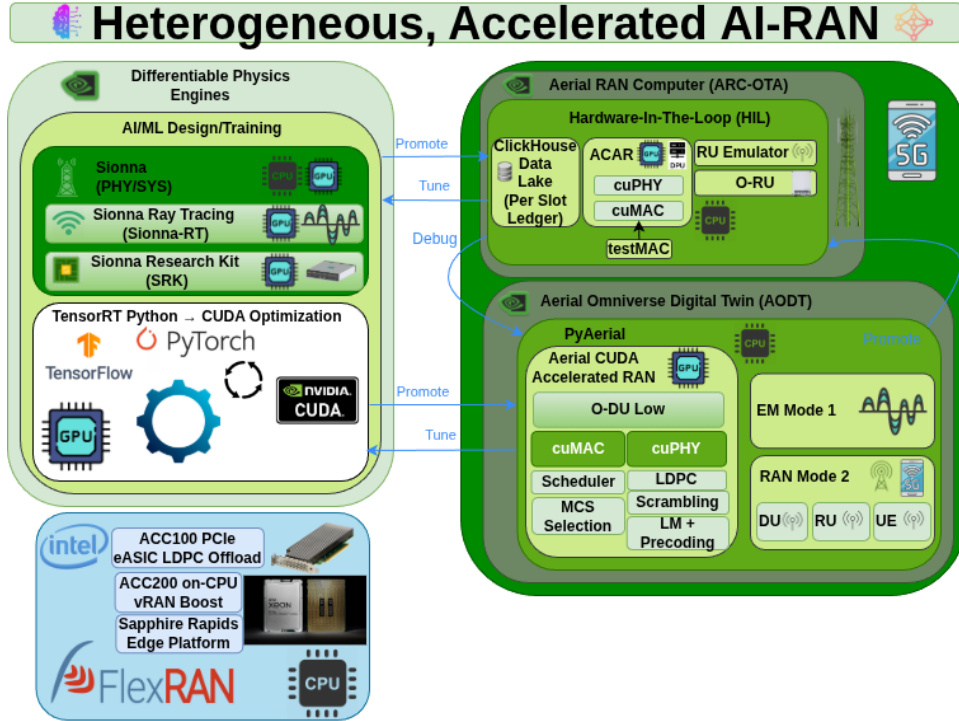


Fig. 2. Heterogeneous, accelerator-aware AI-RAN workflow linking differentiable physics engines (e.g., Sionna/Sionna-RT/SRK) to code-realistic twins and deployment-grade runtimes (e.g., ARC-OTA/ACAR and AODT), enabling promote–tune–debug iteration across offline, twin, and real-time execution.

SYS (system-level simulation via PHY abstraction), while *Sionna-RT* augments these models with differentiable ray tracing for geometry-consistent propagation, built on Mitsuba 3/Dr.Jit [12], [13]. In the *AtlasRAN* taxonomy, Sionna PHY/SYS and Sionna-RT primarily support offline training, evaluation, and channel/data generation that can later be “promoted” into code-realistic twins or real-time stacks.

b) Link-layer emulation and OAI L1 offload—Sionna-RK: The *Sionna Research Kit (Sionna-RK)* targets the transition from offline design to near-RT, system-in-the-loop evaluation by integrating GPU-offloaded PHY components into a running 5G NR stack based on OAI with O-RAN-compliant interfaces [14]. SRK reference workflows include (i) explicit CUDA offload of selected PHY functions (e.g., LDPC decoding), (ii) plugin-style data capture for recording real signals and labels, and (iii) insertion of neural PHY blocks that *can* be deployed via TensorRT for real-time inference when appropriate [14]. Importantly, SRK’s boost is achieved through targeted CUDA implementations integrated into OAI binaries (i.e., not TensorRT “kernel-level optimization” for RAN Digital Signal Processing (DSP) unless TensorRT is used specifically for neural modules), and because SRK is delivered as version-specific patch sets on top of OAI, maintenance may require pinning compatible upstream commits or periodically rebasing/rebuilding the patches as OAI evolves [14]. In Sec. V-D, we observe that SRK’s CUDA LDPC reduces cumulative decoder work relative to CPU-threaded LDPC, yet multi-UE throughput scaling can still collapse under host-OS RF emulation, motivating explicit attention to I/O and timing fidelity alongside kernel acceleration.

c) Deployment compilation: TensorRT: To move trained neural components from research environments into efficient runtime artifacts, NVIDIA’s toolchain uses TensorRT as a deployment compilation step [16]. PyTorch or TensorFlow models are converted into optimized GPU inference engines via operator fusion, precision calibration, scheduling, and memory optimization, producing C++ or Python accessible artifacts. Within the AI-RAN workflow, TensorRT is commonly applied to in-path predictors and learned blocks (e.g., channel estimation and link-quality prediction, learned MCS selection, neural receivers/precoders, and traffic/topology-aware policies), providing a bridge from offline training to GPU-resident inference that can be composed with real-time PHY/MAC kernels [16].

d) ACAR: GPU-native O-DU and fronthaul I/O pathway: ACAR provides a GPU-native runtime for AI-on-RAN by moving key O-DU functions from the CPU to the GPU and SmartNIC. ACAR consists of three tightly integrated components: (i) *cuPHY*, which implements the 5G NR physical layer on the GPU, including FFTs, channel estimation and equalization, LDPC decoding, and MIMO processing; (ii) *cuMAC*, a GPU-based MAC scheduler that supports multi-cell, slot-level scheduling; and (iii) *cuVNF*, an O-RAN 7.2x/eCPRI fronthaul termination and transport pathway designed to minimize CPU involvement by enabling direct NIC-to-GPU data movement and kernel-bypass I/O (e.g., DPDK-based host processing and DOCA GPUNetIO-style delivery into GPU-resident pipelines) [15], [16], [42]–[44]. Because the 7.2x datapath is deadline-driven, ACAR deployments are typically paired with system-level real-time configuration (e.g., CPU isolation, hugepages, VFIO/IOMMU for kernel-bypass device access, and PTP-based synchronization) to stabilize slot-level timing on HPC hosts [44]. ACAR is packaged within the Aerial RAN Computer environment, which exposes *testMAC* and *pyAerial* hooks for driving and instrumenting *cuPHY/cuMAC* (including inserting TensorRT engines or custom CUDA kernels), and can log per-slot telemetry into a ClickHouse-backed ledger to support per-TTI observability consistent with Table I [16].

TABLE I

CAPABILITY MATRIX FOR CHOOSING OPEN 5G/O-RAN/AI-RAN PLATFORMS IN UBIQUITOUS-NETWORK STUDIES. COLUMNS INDICATE REPRESENTATIVE EXECUTION ENVIRONMENTS; ROWS CAPTURE THE MINIMUM PROPERTIES NEEDED TO SUPPORT CLAIMS ABOUT FRONTHAUL BEHAVIOR, CONTROL EXPOSURE, ARTIFICIAL-INTELLIGENCE INSERTION POINTS, AND OBSERVABILITY. **LEGEND:** ✓ = NATIVE OPEN-SOURCE CAPABILITY; × = NOT SUPPORTED IN THE REFERENCED MODE; △ = ACHIEVABLE WITH AUGMENTATION, ADAPTERS, OR THIRD-PARTY INTEGRATION. **NOTE:** THE AERIAL FRAMEWORK (ACAR/AODT) IS ACTIVELY BEING OPEN SOURCED, THOUGH TIMELINES ARE SUBJECT TO CHANGE.

Property / Layer	ns-O-RAN	srsRAN ZMQ	srsRAN-SDR (Split 8)	srsRAN-O-RU/OFH (Split 7.2x)	OAI RFSim	OAI-SDR (Split 8)	OAI-O-RU/OFH (Split 7.2x)	Sionna	Sionna-RT	Sionna-RK	FlexRAN	ACAR	AODT
WG4 7.2x fronthaul (HIL)	×	×	×	✓	×	×	✓	×	×	×	△	✓	×
WG4 7.2x fronthaul (software twin)	×	×	×	×	×	×	×	×	×	×	△	✓	✓
Shared cuPHY & cuMAC GPU kernels	×	×	×	×	×	×	×	×	×	×	×	✓	✓
GPU L1 & slot-deadline MAC	×	×	×	×	×	×	×	×	×	×	×	✓	✓
O-DU-low (hi-PHY + MAC@TTI)	△	△	✓	✓	✓	✓	✓	△	△	×	✓	✓	✓
O-DU-high / O-CU (L2+L3)	△	✓	✓	✓	✓	✓	✓	×	×	✓	✓	△	△
Near-RT E2 loop (E2AP, KPM/RC)	✓	✓	✓	✓	△	△	△	×	×	△	△	△	△
5GC↔UE (out-of-the-box)	×	△	△	△	✓	✓	△	×	×	✓	△	△	△
UE realism (3GPP PHY→NAS attach)	△	△	△	✓	△	✓	✓	×	×	△	✓	△	△
Offline AI-RAN support (AI-for-RAN or AI-and-RAN)	△	△	△	△	△	△	△	✓	✓	△	△	△	△
In-RAN AI (AI-for-RAN or AI-on-RAN)	×	△	△	△	△	△	△	×	×	△	△	✓	✓
Per-TTI observability / ledger	△	△	△	△	△	△	△	×	×	△	△	✓	✓
Typical accessibility	✓	✓	✓	△	✓	✓	△	✓	✓	✓	△	✓	△

Footnote: Columns labeled **.SDR* denote ordinary RF front-end operation, typically corresponding to Split 8 via UHD or comparable SDR radio APIs. Native WG4 7.2x capability, where available, is represented separately under explicit O-RU/OFH columns.

e) AODT: digital twin with shared kernels but different end-to-end I/O: Aerial Omniverse Digital Twin (AODT) complements ACAR by providing a code-realistic digital-twin environment that reuses the same cuPHY/cuMAC kernels, while replacing the deployed fronthaul and timing substrate with simulation/twin components [16], [30]. AODT supports an EM-oriented mode emphasizing high-fidelity ray-tracing propagation and a RAN-centric mode emphasizing protocol-accurate behavior and scaling, but it should not be interpreted as a fully identical end-to-end replica of the ACAR deployment pipeline: its RAN execution is mediated by a slot/event-based simulation layer and does not inherently reproduce the deployed NIC→GPU fronthaul I/O path (e.g., cuVNF with GPUDirect/DPDK/DOCA), host timing/synchronization behavior, or full-stack integration. Instead, AODT typically relies on software RU and UE emulators (with 7.2x-compatible interfaces) and provides similar *testMAC/pyAerial*-style hooks for model insertion, logging, and load testing [16], [30].

f) End-to-end workflow: the three computer framework: Together, these components realize a compact “promotion” loop consistent with Section III-A’s three-computer view: *Computer A* performs differentiable training and dataset generation with Sionna PHY/SYS and Sionna-RT [12], [13]; *Computer B* validates model configurations in a code-realistic twin (AODT) [16], [30]; and *Computer C* executes the resulting components in a real-time, GPU-native O-DU (ACAR) [16], [44]. In practice, researchers can chain Sionna→Sionna-RT→TensorRT→AODT→ACAR, iterating between offline design, twin-based debugging, and in-situ execution as constraints shift from differentiability and throughput to fronthaul I/O, slot deadlines, and per-TTI observability [16].

Enter AI-RAN. To align the terminology subsequently presented, we adopt the AI-RAN Alliance working-group framing [18], [19]: *AI-for-RAN* (“*Enhancing RAN Performance with AI*”) refers to applying AI-driven optimizations to improve RAN spectral/operational efficiency, radio resource management, and predictive maintenance (typically developed and stress-tested in offline or system-in-the-loop environments before deployment); *AI-and-RAN* (“*Shared Infrastructure for AI and RAN*”) refers to the architectural convergence where AI and RAN workloads coexist on shared edge/cloud infrastructure with explicit resource sharing, co-scheduling, and utilization/monetization objectives; and *AI-on-RAN* (“*Running AI at the Network Edge*”) refers to executing AI workloads directly on RAN-resident compute to enable low-latency, in-path inference and edge applications under RAN timing constraints. In *AtlasRAN*, these definitions clarify why “Offline AI-RAN support” and “In-RAN AI” appear as distinct capability dimensions: they separate *where* AI is developed from *where* it must execute, and they motivate treating fronthaul I/O, timing fidelity, and observability as first-class constraints when mapping platforms to experimental goals.

F. Capability Matrix for Ubiquitous-Network Experiment Design

Table I summarizes the *capability matrix* used throughout *AtlasRAN*. We interpret the matrix from the perspective of 5G as ubiquitous infrastructure, where the same platform may be asked to support ground vehicles, roadside edge nodes, or future unmanned-system users under different timing and observability assumptions. The matrix should therefore be read as an experiment-design tool, not a leaderboard: ✓ denotes *native support*, △ denotes support that is *possible with augmentation or external integration*, and × denotes that the property is *not supported* in the referenced mode. SDR-based columns denote ordinary RF front-end operation, typically corresponding to Split 8, whereas native WG4 7.2x capability is represented separately under explicit O-RU/OFH columns. This distinction is essential because the move from SDR substitution to open-fronthaul/O-RU operation introduces synchronization, transport, and RU-capability constraints that materially change what can be claimed about fronthaul behavior, attach realism, and deployment fidelity.

A practical consequence of the split-column presentation is that ordinary SDR execution and native open-fronthaul execution should no longer be treated as interchangeable levels of realism: both can preserve substantial portions of the gNB stack, but only the latter makes RU synchronization, OFH transport, and 7.2x interoperability first-class experimental variables.

- **Control, slicing, and xApps (OSC + near-RT loop).** When the research focus is near-RT control logic (policy updates, slice controls, scheduler knobs) rather than PHY realism, prioritize platforms with native E2 exposure and stable host-OS

iteration loops. REAL exemplifies PPO-based xApp control over an OSC-style near-RT RIC with srsRAN-ZMQ [45], while ORANSlice demonstrates slice-aware scheduling aligned with NVS-style isolation concepts on OAI-based O-DUs [46], [47]. These studies benefit most from per-TTI feature access and repeatable experiment scripting before migrating to SDR/HIL. Because these studies primarily depend on E2 exposure and repeatable control-plane iteration, they usually benefit more from stable host-OS or software-only execution than from immediate migration to SDR or O-RU/OFH modes.

- **Sim-to-HIL progression (ns-O-RAN → emulation → SDR/HIL → O-RU/OFH).** For algorithm development that must eventually face RF and fronthaul constraints, a staged workflow reduces iteration cost: (i) prototype at scale in ns-O-RAN (control-plane abstractions, large topologies), then (ii) validate protocol interactions in host-OS emulation (OAI RFSim or srsRAN-ZMQ), then (iii) move to ordinary SDR-based HIL for Split 8-style RF execution, and finally (iv) exercise native WG4 7.2x HIL through explicit O-RU/OFH paths when fronthaul timing, synchronization, and RU interoperability become part of the claim. Shared infrastructures—including Colosseum/OpenRAN Gym, X5G, OAIC, 6G-SANDBOX, and POWDER—provide later-stage RF, orchestration, and multi-node experimentation resources, though the level of exposed fronthaul realism varies substantially across them: some emphasize SDR operation and massive channel emulation, whereas others additionally provide O-RAN-specific fronthaul, O-RU testing (e.g. Open RAN Studio and Keysight RuSIM over 7.2 OFH) or hosted open-RAN deployment facilities [8]–[11], [48].
- **Shared-infrastructure mobility studies.** When the research question assumes that road users and other mobility clients share the same 5G infrastructure, platform choice should be driven by the strongest realism requirement in the loop. Network-wide policy and orchestration studies may begin in ns-O-RAN or host-OS emulation, claims involving RF execution may move to Split 8 SDR-based HIL, and claims involving fronthaul timing, synchronization, RU interoperability, or open-fronthaul transport should move further to explicit O-RU/OFH deployments, code-realistic twins, or GPU-native runtimes with explicit observability and transport semantics.
- **End-to-end DRL scheduling with protocol realism (software-only → SDR/O-RU).** If the target is closed-loop scheduling under NR signaling and a functioning core-network path, select platforms with deeper RAN/core integration (rows “O-DU-high/O-CU” and “5GC↔UE”). DORA illustrates DRL-driven scheduling in an OAI-based environment where full-stack behavior and instrumentation can be exercised prior to over-the-air variability [49]. Where the claim extends beyond protocol realism to RF execution or open-fronthaul behavior, the evaluation should progress from software-only environments to Split 8 SDR or explicit O-RU/OFH modes as appropriate.
- **Differentiable PHY and dataset generation (Offline AI-RAN).** For learned receivers/precoders/channel models and scaled data generation, use Sionna PHY/SYS and Sionna-RT (row “Offline AI-RAN support”), where differentiability and GPU batch throughput dominate design constraints [12], [13].
- **Near-RT GPU offload inside open-source stacks (bridge to online AI-for-RAN and AI-on-RAN).** When the goal is to prototype GPU acceleration or AI blocks *inside* a familiar open-source RAN codebase while retaining O-RAN-facing interfaces, SRK provides a practical bridge (column “Sionna-RK”): selective CUDA offload, integrated capture, and optional TensorRT deployment for neural modules, at the cost of version-sensitive patch management [14].
- **Accelerator-backed scaling and heterogeneous resource partitioning (traditional acceleration → AI-RAN).** To study how fixed-function acceleration changes achievable bandwidth/cell density and frees CPU headroom for control and AI tasks, FlexRAN and CloudRIC-style deployments are canonical references, capturing FEC/PHY offload via ACC100/ACC200/vRAN-Boost classes of acceleration and the resulting trade-offs [15], [39], [41]. These studies are often strongest when the compute path itself is the object of analysis, exemplified by Six Times to Spare [7], and thus do not automatically require native O-RU/OFH execution unless the claim depends explicitly on open-fronthaul transport or RU-coupled timing behavior.
- **GPU-native online AI-RAN with digital twins (AODT ↔ ACAR).** For experiments that require GPU L1, slot-deadline MAC, and per-TTI ledgers—and that explicitly evaluate promotion from offline training to twin-based debugging to real-time execution—AODT and ACAR form a direct pipeline (rows “GPU L1 & slot-deadline MAC” and “Per-TTI observability”) [16], [30], [44]. This archetype is appropriate when the research question depends on in-path inference, GPU scheduling interactions, and fronthaul I/O constraints rather than purely offline model quality.

IV. EXPERIMENTAL METHODOLOGY

A. Objective and Compute-vs-Harness Ablation

To demonstrate how *AtlasRAN* proactively mitigates invalid comparisons, we present a rigorous CU–DU load evaluation in which a commonly used host-OS emulation yields non-physical multi-UE scaling under UE concurrency; this is a capability-matrix “stress test” that ties functional labels (e.g., software fronthaul emulation, host scheduling, and observability) to concrete measurement artifacts and shows that timing and I/O fidelity must be treated as first-class experimental variables rather than incidental details. The scenario is representative of a shared ubiquitous-network edge node: a common 5G infrastructure element that may need to serve multiple user devices while preserving headroom for higher-layer vehicular or other unmanned-system services.

To showcase actionable results, the evaluation isolates how a *host-OS emulation harness* can dominate multi-UE scaling KPIs even when underlying PHY is held fixed: the goal is not to claim one stack is “faster”, but to demonstrate why timing and I/O fidelity must be first-class when reporting goodput under UE concurrency. Concretely, we compare baseline OpenAirInterface (OAI) in RFSim mode against Sionna Research Kit (SRK), which offloads LDPC decoding to CUDA while preserving the surrounding OAI execution path, enabling a targeted compute-vs-harness ablation. Both baselines run on a single NVIDIA DGX Spark (Grace CPU + Blackwell GPU, 128 GB NVLink-C2C coherent memory), providing a common CPU/GPU/memory harness and minimizing CPU↔GPU data-movement confounds when interpreting SRK’s CUDA offload. This is the practical bridge to the shared-infrastructure framing: a platform that appears sufficient for single-user protocol validation may still be inadequate for studying shared-infrastructure scaling due to inter-process communication (IPC) limitations.

B. System Model, Workload, and Measurement Pipeline

Our experiment uses a split OAI SA gNB with an F1 CU–DU decomposition and an RFSim DU that replaces RU/OTA behavior with a software-based AWGN channel abstraction rather than a fronthaul-faithful endpoint. To reduce host-OS scheduling variance, we pin the OAI-NR-CU and OAI-NR-DU to disjoint CPU core sets (CU: 6–7; DU: 8–11), leaving remaining cores for UE containers and monitoring. For each UE count $N \in \{1, 3, 6, 12\}$, we run a 60s saturated uplink TCP load test using `iperf3` with one flow per UE and aggregate throughput computed at the DN receiver. Throughout this section, “ZMQ” refers to an external KPI/xApp transport used to stream KPM-like telemetry to a subscriber during the run (not srsRAN’s “ZMQ radio mode”), and it is treated as part of the instrumentation harness whose stability under load matters for claims about near-RT control and observability.

Fig. 3 summarizes the end-to-end test harness and the instrumentation used to generate the measurements reported in this section. We sample CU and DU CPU utilization at 0.5s granularity via `docker stats`, and for SRK runs we additionally sample GPU utilization and power via `nvidia-smi`. In parallel, we follow CU/DU logs to extract LDPC timing, collect per-UE `iperf3` JSON outputs, and record the ZMQ KPI stream; all artifacts are then consolidated per-run and per-environment into the summarized KPIs in Table II.

C. Utilization Semantics and Core-Equivalent Normalization

Throughout this analysis, CPU utilization is interpreted in *core-equivalent* units: 100% corresponds to one fully utilized logical CPU (one core worth of work). This is the convention used by common per-process/container tools (e.g., `top` in IRIX mode and `docker stats`), so values may exceed 100% on multicore systems. In our harness, the DU container is pinned to four cores (cores 8–11) and the CU container is pinned to two cores (cores 6–7), so their theoretical maxima are 400% and 200%, respectively. For intuition, 350% should be read as “ ≈ 3.5 cores” (and, for the DU, $\approx 87.5\%$ of its pinned 4-core budget). We report an additional host-wide CPU metric (`SYS CPU`) to avoid conflating “high DU CPU” with global CPU exhaustion: `SYS CPU` is measured at the host level and expressed on the same core-equivalent scale so it can be compared directly against CU/DU container CPU.

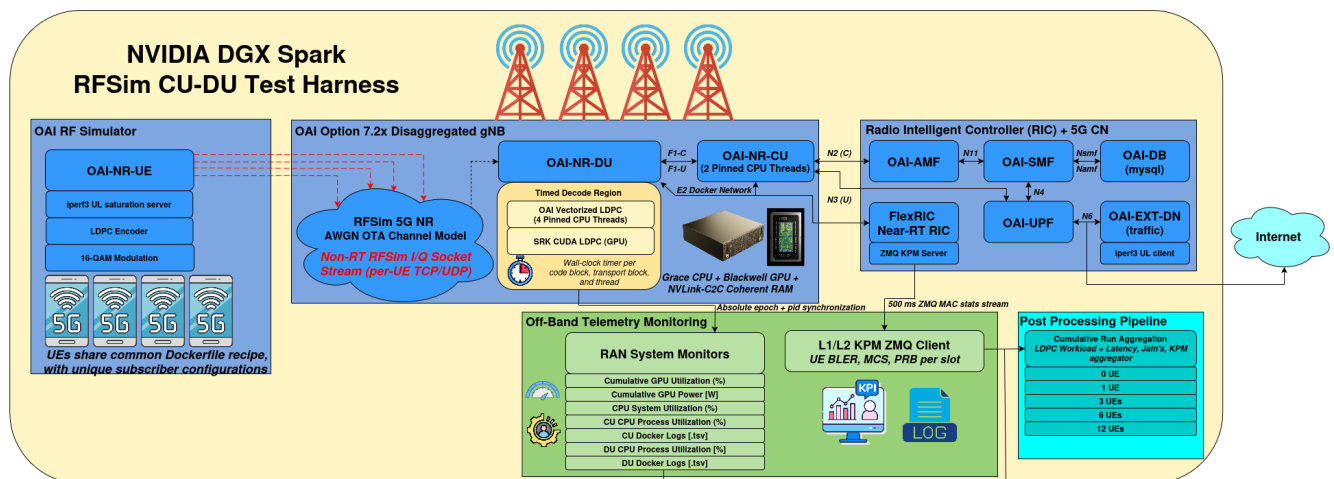


Fig. 3. CU–DU ablation architecture and monitoring pipeline for the RFSim load study on a common NVIDIA DGX Spark host (Grace CPU + Blackwell GPU, 128 GB NVLink-C2C coherent memory). The DU runs OAI RFSim (UE/RU-PHY abstraction) and exchanges F1 control/user-plane traffic with the CU; we compare baseline OAI (vectorized CPU LDPC) against SRK (CUDA LDPC) with wall-clock timing instrumentation around the decode region. CU/DU threads are pinned to fixed CPU core sets (CU: 6–7; DU: 8–11). Uplink load is generated by `iperf3` and KPIs are exported over a ZMQ monitor to an xApp-style subscriber before post-processing. **This figure depicts a host-OS emulation harness intended for controlled ablations, not a fronthaul-faithful software/cyber-physical twin.**

Because RFSim removes OTA uncertainty and exposes a software-controlled channel model, single-UE uplink goodput should be close to a modulation/bandwidth-limited upper bound given the configured PRBs and the MCS actually selected by the scheduler (we observe 16-QAM, i.e., $Q_m = 4$). We therefore define a compact *raw payload* bound (before DMRS/control, coding, and stack overhead) as

$$R_{\text{raw}} \approx N_{\text{PRB}} \cdot N_{\text{sc}} \cdot N_{\text{sym}} \cdot f_{\text{slot}} \cdot Q_m, \quad (1)$$

where $N_{\text{PRB}} = 106$ PRBs, $N_{\text{sc}} = 12$ subcarriers/PRB, $N_{\text{sym}} = 14$ OFDM symbols/slot, and $f_{\text{slot}} = 2000$ slots/s for 30 kHz SCS. Plugging these constants yields $R_{\text{raw}} \approx 142.46$ Mbps, and we map measured 1-UE goodput to an efficiency η via $T(1) = \eta R_{\text{raw}}$: OAI achieves 114.59 Mbps ($\eta \approx 0.80$) and SRK achieves 103.34 Mbps ($\eta \approx 0.73$), indicating that both stacks operate near the bandwidth/MCS ceiling in the absence of UE concurrency. SRK’s lower efficiency appears as an artifact of I/O limitations despite increased workload efficiency, as we will unpack across multiple vectors throughout this analysis.

V. MEASUREMENT RESULTS

A. CU-DU Performance Evaluation

Fig. 4 reports the headline result: aggregate uplink goodput T_{total} versus UE count N for both baselines, and Table II summarizes the full KPI set (throughput, fairness, utilization, and LDPC timing). LDPC times in Table II come from in-

TABLE II

CORE KPIS FOR THE CU–DU LOAD STUDY (EACH ENTRY: MEAN/P95 OVER 0.5 S STEADY-STATE SAMPLES FROM A 60 S RUN). CPU UTILIZATION IS REPORTED IN *core-equivalent* UNITS (100% \equiv ONE LOGICAL CORE), SO VALUES MAY EXCEED 100%; DU AND CU CONTAINERS ARE PINNED TO 4 AND 2 CORES (MAX 400% AND 200%). SYS CPU IS HOST-WIDE CPU ON THE SAME SCALE. “LDPC/TW” AND “LDPC CUM” ARE IN-CODE MICROSECOND WALL-CLOCK TIMINGS AROUND THE LDPC DECODE CALL (CPU: CLOCK_MONOTONIC_RAW; SRK: CUDA TIMING). “LDPC CUM” IS AN ESTIMATED PER-TB CUMULATIVE DECODER COST: OAI USES A CORE-TIME PROXY ($t_{\text{OAI}}^{\text{cum}} = 4 t_{\text{OAI}}^{\text{call}}$); SRK EQUALS THE SINGLE CUDA CALL. GPU UTILIZATION/POWER ARE REPORTED FOR SRK ONLY.

N	T_{total}		$T_{\text{per-UE}}$		Jain J		DU CPU (core-equiv. %)		CU CPU (core-equiv. %)		SYS CPU (core-equiv. %)		LDPC/thread (μs)		LDPC cum (μs)		SRK GPU (util% / W)	
	OAI	SRK	OAI	SRK	OAI	SRK	OAI	SRK	OAI	SRK	OAI	SRK	OAI	SRK	OAI	SRK	util	power
0	NA	NA	NA	NA	NA	NA	210.16/213.27	212.87/216.09	1.71/2.29	1.87/2.84	305.6/336.6	301.6/340.0	79.87/91.10	NA	79.87/91.10	NA	1.29/3.70	11.48/12.11
1	114.59	103.34	114.59	103.34	1.000000	1.000000	324.79/326.77	349.31/351.64	22.98/24.43	20.73/22.54	534.6/561.6	557.2/594.8	255.86/262.09	316.02/350.83	1016.74/1048.36	316.02/350.83	44.85/47.00	38.48/39.11
3	65.21	66.44	21.74	22.15	0.999997	1.000000	289.93/291.73	329.73/339.57	16.80/17.68	17.21/18.11	502.2/527.4	585.0/636.4	262.60/268.36	316.90/347.89	1042.06/1073.45	316.90/347.89	29.28/34.00	29.73/30.54
6	35.09	35.01	5.85	5.84	0.999484	0.999930	205.54/207.18	231.60/244.69	9.02/10.63	9.77/10.75	391.6/428.6	484.6/521.6	275.27/286.05	369.47/392.66	1087.42/1144.18	369.47/392.66	19.34/22.00	22.25/23.14
12	16.35	16.15	1.36	1.35	0.999997	0.999998	162.38/164.92	172.91/176.62	5.69/6.89	5.80/6.78	338.2/359.0	389.2/414.0	273.18/293.63	345.17/373.05	1063.82/1174.53	345.17/373.05	9.45/11.00	17.08/17.60

code instrumentation around the decoder call (e.g., CPU: `clock_gettime(CLOCK_MONOTONIC_RAW)`; SRK: CUDA-side decode timing), not from external coarse-grained sampling. Despite near-ceiling single-UE performance, both stacks exhibit a steep and smooth collapse under UE concurrency: OAI drops from 114.59 Mbps at $N=1$ to 16.35 Mbps at $N=12$ (a $7.01\times$ reduction), while SRK drops from 103.34 Mbps to 16.15 Mbps ($6.40\times$). On a log–log scale the data is well explained by a simple power law, with $T_{\text{OAI}}(N) \approx 129.08 \cdot N^{-0.7759}$ ($R_{\log}^2=0.9668$) and $T_{\text{SRK}}(N) \approx 120.07 \cdot N^{-0.7406}$ ($R_{\log}^2=0.9446$), suggesting a shared scaling clamp rather than a sharp saturation threshold isolated to one decoder implementation.

Table II also includes an explicit $N=0$ (idle) baseline that isolates harness overhead before any uplink PHY work is introduced: even with no active UEs, the pinned DU process consumes ≈ 210 – 213% CPU while the host-wide SYS CPU (single-core equivalent, assuming 20 cores) remains ≈ 302 – 340% (i.e., ≈ 3.0 – 3.4 cores), and the DU advances faster than real time (slot rate $> 3\times$ nominal, with real-time factor $\text{RTF} \triangleq \frac{\text{observed slot-processing rate}}{\text{nominal slot rate}}$ satisfying $\text{RTF} > 3$), anchoring the interpretation that RFSim host-OS emulation can “run ahead” when unconstrained. Turning on a single saturated uplink flow ($N=1$) loads the full receive chain and activates LDPC decoding, which immediately raises DU CPU to 324.8% (OAI) / 349.3% (SRK), increases CU CPU from $\approx 2\%$ to ≈ 21 – 23% , and lifts SYS CPU to ≈ 535 – 595% (i.e., ≈ 5.3 – 6.0 cores) while slowing the slot progression (RTF drops to 1.84 for OAI and 1.70 for SRK). This transition also makes the compute ablation visible in the timing and accelerator counters: OAI’s LDPC region reports 255.9 μs per thread with an estimated cumulative core-time proxy of 1.02 ms per transport block, whereas SRK’s CUDA decoder reports 316 μs per transport block while driving the GPU from near-idle (1.3% util, 11.5 W at $N=0$) to sustained load (44.9% util, 38.5 W at $N=1$), showing that the step from $N=0 \rightarrow 1$ is dominated by the active uplink pipeline (including LDPC decode) rather than background monitoring overhead.

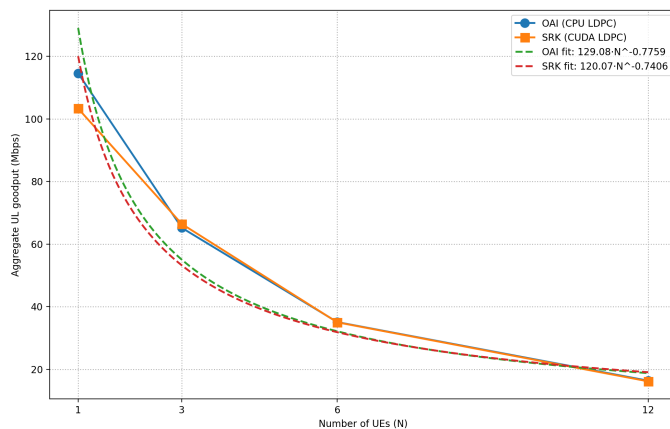


Fig. 4. Headline result: aggregate UL goodput T_{total} vs. UE count $N \in \{1, 3, 6, 12\}$ for OAI (CPU LDPC) and SRK (CUDA LDPC), with power-law overlays fitted in log space. Fits: $T_{\text{OAI}}(N) \approx 129.08 \cdot N^{-0.7759}$ ($R_{\log}^2=0.9668$) and $T_{\text{SRK}}(N) \approx 120.07 \cdot N^{-0.7406}$ ($R_{\log}^2=0.9446$).

B. Fairness Under Concurrency: Ruling Out UE Starvation

To differentiate “scheduler unfairness” from “system-wide throughput clamp,” we compute Jain’s fairness index over per-UE `iperf3` throughputs, $J = \frac{(\sum_i x_i)^2}{n \sum_i x_i^2}$, where x_i is the goodput of UE i . Fairness remains essentially perfect at higher loads—OAI $J=0.999484$ at 6 UEs and 0.999997 at 12 UEs, and SRK $J=0.999930$ at 6 UEs and 0.999998 at 12 UEs—so the collapse is not explained by a few UEs being starved while others dominate. Instead, each UE’s share drops roughly proportionally with N (e.g., OAI from ≈ 114.59 Mbps/UE at $N=1$ to ≈ 1.36 Mbps/UE at $N=12$), consistent with uniform bottlenecking that slows the experiment time-scale and throttles the uplink pipeline.

In a compute-bound RAN, adding UEs increases the arrival rate of transport blocks to the DU, so DU CPU (and, with offload, GPU) utilization typically rises. In RFSim host-OS emulation, however, multi-UE concurrency can reduce the *delivered* workload due to non-real-time I/Q transport behavior (socket contention, queuing, and time-scale dilation). A simple relation makes the directionality explicit:

$$U_{\text{LDPC}} \propto \lambda_{\text{TB}} t_{\text{LDPC}}^{\text{cum}}, \quad (2)$$

TABLE III
DERIVED CONSTANTS AND FITTED MODEL PARAMETERS FOR THE CU-DU LOAD STUDY (RFSIM HOST-OS EMULATION).

Quantity	Value
Configured PRBs	$N_{\text{PRB}} = 106$
Subcarriers/PRB	$N_{\text{sc}} = 12$
Symbols/slot	$N_{\text{sym}} = 14$
Slot rate (30 kHz SCS)	$f_{\text{slot}} = 2000$ slots/s
Observed modulation	$Q_m = 4$ (16-QAM)
Raw UL payload bound	$R_{\text{raw}} \approx 142.46$ Mbps (Eq. 1)
Single-UE goodput	OAI: 114.59 Mbps ($\eta \approx 0.80$); SRK: 103.34 Mbps ($\eta \approx 0.73$)
Log-fit power laws	$T_{\text{OAI}}(N) \approx 129.08 \cdot N^{-0.7759}$ ($R_{\text{log}}^2 = 0.9668$) $T_{\text{SRK}}(N) \approx 120.07 \cdot N^{-0.7406}$ ($R_{\text{log}}^2 = 0.9446$)
Collapse (1→12 UE)	OAI: 7.01×; SRK: 6.40×
SRK GPU energy proxy	P_{GPU}/T : 0.37 W/Mbps (1 UE) → 1.06 W/Mbps (12 UE)

where λ_{TB} is the number of decoded transport blocks per *wall-second* and $t_{\text{LDPC}}^{\text{cum}}$ is the per-transport-block cumulative decoder time. In our data, $t_{\text{LDPC}}^{\text{cum}}$ remains roughly stable across N (Table II), while λ_{TB} collapses alongside goodput and the experiment time-scale (RTF), so the observed CPU/GPU utilization drops. Under this interpretation, decreasing utilization is not an arithmetic error; it is a symptom that the pipeline is being under-fed upstream of the decoder. Because the uplink generator uses TCP (`iperf3`), transport backpressure and retransmissions under RFSim congestion also reduce the effective offered rate, further lowering the arrival rate of decodable work at the DU. Attempting unbounded UDP floods or alternative DPDK/accelerated traffic generators (e.g., Keysight `ixia-c.dev` [50]) upon RFSim’s transport frequently results in server or process death, corrupting the channel. We therefore gauge socket health through TCP monitoring.

The utilization traces reinforce this interpretation. If multi-UE collapse were driven by decoder saturation, we would expect DU CPU (and for SRK, GPU) utilization to *increase* with N as the system struggles to keep up; we observe the opposite. OAI DU CPU mean decreases from 324.8% at 1 UE to 162.4% at 12 UEs, and SRK DU CPU mean decreases from 349.3% to 172.9% over the same range (Table II); corresponding p95 values also decrease. SRK GPU utilization and power fall sharply, from 44.9% and 38.48 W at 1 UE to 9.4% and 17.08 W at 12 UEs, indicating that the accelerator is increasingly *under-fed* rather than over-subscribed, even given the coherent-memory harness.

C. High-Load Data Quality Notes

The $N=12$ utilization point in Table II should be interpreted conservatively because the corresponding `iperf3` JSON logs are partial: at this UE scale, connection can become intermittent, RRC instability can occur, and individual `iperf3` connections can be lost momentarily within communications as the RFSim I/Q transport socket stream collapses and the harness time-scale dilates. During our tests, we noted all twelve UEs remained connected and `iperf3`’s client/server did not crash; however, the JSON outputs reflect incomplete measurements (e.g., missing end-of-test summaries), which can bias both throughput and windowed KPI aggregation and therefore contribute to the appearance of smaller CPU utilization at $N=12$. In contrast, the $N \in \{0, 1, 3, 6\}$ runs are fully measured end-to-end in `iperf3`, so their CPU/GPU KPI windows provide a more complete representation of steady-state load.

Including SYS CPU (host-wide cumulative CPU utilization) alongside per-container CU/DU CPU resolves the otherwise paradoxical observation that DU CPU decreases as UE count increases: with SYS CPU expressed on the same single-core scale (host%×20), the system remains far from saturated throughout the study (e.g., ≈ 302 – 340% at $N=0$ while the DU container burns ≈ 210 – 216% CPU on pinned cores), indicating substantial host headroom outside the CU/DU core sets and anchoring the conclusion that “high DU CPU%” does not imply global CPU exhaustion. More importantly, SYS CPU co-varies with timing fidelity: as UE concurrency increases, the observed slot-processing rate collapses and RTF falls from > 1 at $N=1$ to ≈ 0.28 at $N=12$, and SYS CPU correspondingly drops (OAI: 534.6% → 338.2%; SRK: 557.2% → 389.2%), demonstrating time-dilation (less effective work per wall-second) rather than resource saturation as the dominant driver of the multi-UE goodput collapse. This system-level view also strengthens the compute ablation result: even where SRK reduces the LDPC work per transport block by roughly $3\times$ relative to OAI’s cumulative CPU proxy (OAI ≈ 1.06 – 1.09 ms vs. SRK ≈ 0.32 – 0.37 ms at $N=6$ – 12), aggregate goodput remains nearly identical at those points, reinforcing that the limiting factor in this host-OS emulation harness is timing/I/O fidelity upstream of the decoder rather than LDPC throughput itself.

D. LDPC Decode Micro-Timing: CPU SIMD/MIMD vs CUDA Offload

To make the compute ablation explicit, we next examine LDPC decode timing extracted from DU logs. In baseline OAI, LDPC decoding for the PUSCH receive chain is reached through the `nrLDPC_coding_interface` and invoked in the UL SCH path as a single call to `nrLDPC_coding_decoder(&slot_parameters)`. This call encapsulates the segment-wise (code-block) 5G NR LDPC belief-propagation decode for the selected basegraph (BG1/BG2) after rate-matching has determined the number of code-block segments, C_{total} , to be processed in the current slot. In the CPU backend, OAI combines MIMD and SIMD: segments are decoded concurrently as independent tasks across the DU thread pool, while each worker executes SIMD-vectorized CN/VN update kernels. The DU log line therefore reports the *wall-clock* duration of this parallel decode region and a per-segment normalization, rather than an end-to-end RX-chain timing. To compare CPU and GPU *work* on a common footing, we additionally report a cumulative CPU core-time proxy defined as $t_{\text{OAI}}^{\text{cum}} \triangleq N_{\text{thread}} \cdot t_{\text{OAI}}^{\text{call}}$, where $N_{\text{thread}} = 4$ is the configured CPU LDPC worker parallelism used in our DU runs; this proxy upper-bounds the total LDPC core- μs and becomes tight when the worker pool is fully busy for the full call duration.

In SRK, the LDPC stage is replaced by NVIDIA’s CUDA-based decoder: an iterative min-sum BP implementation that alternates `update_cn_kernel` and `update_vn_kernel` over compact BG tables using `int8` message/accumulator buffers with explicit damping and clipping, and produces packed hard decisions via `pack_bits_kernel` on a per-thread CUDA stream; on unified-memory platforms, input LLRs can be staged in pinned, host-mapped buffers (e.g., `cudaHostAllocMapped`) to minimize transfer overhead. Consequently, SRK exposes one GPU-side timing per transport block (per decode invocation), for which “per-call” and cumulative cost coincide. Across UE counts, OAI’s mean per-call decode time remains in the 256–277 μs range, but $t_{\text{OAI}}^{\text{cum}}$ ($4\times$ parallelism) is 1.03–1.11 ms, while SRK’s CUDA decode time is 319–343 μs . The cumulative LDPC work ratio (OAI/SRK) is therefore $\approx 3.2\times$, yet the throughput collapse is of comparable magnitude for the two stacks, strengthening the claim that the limiting factor lies outside the decoder kernel itself.

Fig. 5 presents a representative excerpt from the OAI DU log stream for the 12 UE experiment captured in `runs/20260219_174039_ues12/`. Concretely, our instrumented implementation wraps the decoder call inside `nr_ulsch_decoding.c`, taking timestamps via `clock_gettime(CLOCK_MONOTONIC_RAW)` immediately before and after `nrLDPC_coding_decoder(&slot_parameters)`. For each invocation, it computes the total decoded segment count C_{total} by summing TBs `[pusch_id].C` across the active PUSCH allocations in the slot, atomically accumulates (i) elapsed nanoseconds, (ii) segment counts, and (iii) call counts across threads, and rate-limits prints to ≈ 1 Hz using an atomic compare-exchange on a `last_log_ns` guard. Thus, each CPU LDPC decoder line is an average over an $\mathcal{O}(1\text{s})$ window; the parenthesized `us/seg` term is the corresponding per-segment mean. For transparency, the exact `du_logs.tsv` lines emitted in simulation are displayed with corresponding pre-appended absolute timestamps.

```

...
1772062027043 oai-nr-du 532641.987492 [NR_PHY] I CPU LDPC decoder: 235.07 us ( 59.18 us / seg)
1772062028044 oai-nr-du 532642.988237 [NR_PHY] I CPU LDPC decoder: 245.17 us ( 54.72 us / seg)
1772062029045 oai-nr-du 532643.989153 [NR_PHY] I CPU LDPC decoder: 259.67 us ( 47.00 us / seg)
1772062030045 oai-nr-du 532644.989275 [NR_PHY] I CPU LDPC decoder: 229.60 us ( 34.58 us / seg)
1772062030875 oai-nr-du 532645.818719 [NR_MAC] I Frame.Slot 768.0
...

```

Fig. 5. Representative excerpt from the OAI DU log stream showing successive CPU LDPC decoder timing prints (extracted verbatim from `du_logs.tsv`; ellipses denote omitted surrounding lines). Each print reports the average wall-clock latency of `nrLDPC_coding_decoder(&slot_parameters)` over a rate-limited window. In the CPU backend, this call implements a MIMD \times SIMD strategy: code-block segments are dispatched as independent tasks onto the DU thread pool (4 workers in our runs), while each worker executes SIMD-vectorized belief-propagation (CN/VN) update kernels. The parenthesized value normalizes the measured wall-clock latency by the decoded code-block segment count; because segments are processed in parallel, this per-segment value is a convenience throughput/normalization metric rather than the serial latency of a single segment.

E. CU-DU Synthesis: Instrumentation Under Stress

Beyond compute and goodput, auxiliary monitors expose a second harness-level symptom under high concurrency: the measurement/control-plane can stall even when fairness remains high among the active UEs. In our ZMQ KPI/xApp telemetry, the subscriber receives a stable stream at moderate UE counts (on the order of 10^2 messages/s in 6-UE runs), but at 12 UEs the stream drops to zero messages, consistent with backpressure or scheduling starvation in the host-OS pipeline rather than a protocol-level scheduling pathology. The traffic generator reflects this stress as well: SRK’s `iperf3` success rate declines to 0.833 at 12 UEs (some flows terminate early), even though the UEs that remain active still share throughput fairly ($J \approx 1$).

Taken together, these observations point to a shared upstream clamp that dominates both baselines: the CU–DU–UE experiment time-scale and I/O path provided by RFSim host-OS emulation. RFSim explicitly trades real-time guarantees for convenience—Eurecom documents that it “*works like an RF board, but not in real-time,*” and can run faster or slower depending on CPU availability [23]. Under multi-UE load, the interaction between OS scheduling, user-space transports, buffering, and the RFSim sample-forwarding model can therefore throttle the end-to-end pipeline (and even stall telemetry), causing both CPU and GPU resources to idle while goodput collapses. This is precisely the regime where accelerating one kernel (LDPC) does not recover scaling, because the bottleneck shifts from compute to timing/I/O fidelity in the harness. In RFSim host-OS emulation, compute acceleration reduces per-TB decode cost but does not restore multi-UE scaling because the dominant limiter is time-coupling and I/Q transport fidelity.

For *AtlasRAN*, the implication is not that RFSim is “wrong,” but that it must be classified, and used, as host-OS emulation: valuable for functional integration (xApp prototyping, instrumentation, regression testing, and controlled micro-ablation studies), yet risky as evidence for multi-UE scaling claims that are sensitive to real fronthaul and slot-deadline dynamics. A timing-faithful software or cyber-physical twin would need explicit, measurable couplings (live bidirectional exchange with known synchronization properties) and engineered time discipline across components [5]; at scale, this typically implies PTP-synchronized pipelines and transport paths designed to preserve deadline behavior under load [6]. Our case study is a concrete “matrix stress test” motivating the selection guidance in Table I: when the research question depends on scaling KPIs, platform choice must privilege timing and I/O fidelity at least as much as protocol completeness or kernel acceleration.

From the perspective of ubiquitous-network evaluation, the key result is not merely that goodput decreases with load. The more important result is diagnostic: fairness stays near ideal while compute demand falls, which means the platform is not revealing a clean scheduler or decoder limit. It is revealing a harness limit. For shared-infrastructure studies, this distinction matters because misleading scalability results can propagate into incorrect conclusions about edge dimensioning, control-loop stability, or the apparent benefit of AI and acceleration.

VI. DISCUSSION

The central implication of *AtlasRAN* is that, once 5G is framed as a ubiquitous communication substrate for connected road vehicles, roadside infrastructure, and future unmanned-system services, platform selection becomes part of the modeling

problem rather than a secondary implementation detail. In this sense, O-RAN is valuable to *AtlasRAN* not merely as an open implementation ecosystem, but as the interface structure that forces timing, fronthaul, control, and anchoring assumptions to be declared. Experimental validity depends on matching the evaluation environment to the strongest timing and coupling requirement in the claim. Simulation and host-OS emulation may be entirely appropriate for xApp logic, orchestration, network slicing, or high-level mobility studies. However, when the claim concerns shared edge bottlenecks, fronthaul timing, slot-level interactions between radio processing and online inference, or multi-domain contention across heterogeneous mobility users, those same environments may be insufficient.

a) *The journey toward cyber-physical systems.*: This perspective places open 5G experimentation on a progression from interface-compatible software models to cyber-physical systems (CPSs). The progression is not simply “simulation versus hardware”; it runs from simulation, to emulation, to software twins, to digital twins, and finally to CPSs in which the digital and physical domains are explicitly coupled. In this context, Twi-Net is especially instructive because it argues that a twin becomes truly cyber-physical only when bidirectional coupling and measurable timing semantics are part of the experimental contract, rather than merely the protocol interface [5]. AutoRAN reinforces the same systems lesson from a complementary direction: when RAN control, data, acceleration, and networking resources are scaled under load, timing, transport, and specialized interconnect behavior must be treated as first-class design variables rather than hidden implementation details [6]. Taken together, these works sharpen a distinction that is essential for ubiquitous-network research: *interface-compatible* is not the same as *time-faithful*, and that difference becomes decisive as experiments move closer to deployment claims.

b) *AtlasRAN’s Contribution.*: The case study in Section IV makes this progression concrete. Under radio-frequency simulation (RFSim) host-OS emulation, aggregate uplink throughput collapses by approximately 6–7 \times as the number of user devices (UEs) increases from 1 to 12 in both stacks (OpenAirInterface (OAI): 7.01 \times ; Sionna Research Kit (Sionna-RK): 6.40 \times), even though fairness remains approximately 1 and both central processing unit (CPU) and graphics processing unit (GPU) utilization decrease rather than increase. This is not the signature of a saturated physical layer (PHY). It is the signature of time-scale dilation and online input/output (I/O) starvation in an under-fed pipeline. In other words, once a major decoder bottleneck is reduced, the dominant limit can move outward to the surrounding transport and timing harness. That is the specific performance-evaluation contribution of *AtlasRAN*: it shows how a platform can preserve functional correctness yet still distort scaling conclusions when time coupling is weak.

This matters directly for shared-infrastructure studies because edge nodes are expected to support more than baseband processing alone. The same node may need to host cooperative perception, mobility coordination, safety analytics, or other higher-layer services while still sustaining radio deadlines. In that setting, coherent CPU–GPU memory and accelerator offload are valuable because they reclaim CPU headroom and rebalance work away from the host. But *AtlasRAN* shows that reclaimed compute headroom does not automatically translate into better end-to-end scaling. If the software harness cannot feed the accelerated path at the required rate, then the experiment becomes I/O-limited, and the apparent bottleneck shifts away from the kernel that was optimized.

For this reason, future studies of ubiquitous 5G infrastructure should report four classes of experimental variables alongside conventional key performance indicators (KPIs): (i) the execution regime used for the study, such as simulation, emulation, software twin, digital twin, or hardware-in-the-loop (HIL); (ii) the timing discipline enforced across components, including synchronization, jitter tolerance, and deadline behavior; (iii) the transport and memory path between major processing stages; and (iv) the level of per-slot or per-interval observability available during execution. We further argue that authors should state explicitly whether a claim is merely interface-compatible or genuinely time-faithful. Without this information, results on scalability, near-real-time behavior, or shared-infrastructure efficiency can be misinterpreted.

Seen in this light, the journey toward cyber-physical systems is not merely a matter of adding hardware or increasing protocol completeness. It is a progression toward tighter timing, richer observability, and more explicit coupling among computation, transport, and the physical environment. Twi-Net, AutoRAN, and *AtlasRAN* converge on this systems lesson from different directions: trustworthy wireless-systems evidence requires experimental stacks whose timing and I/O semantics are commensurate with the claims being made [5], [6]. For 5G as a ubiquitous network supporting vehicular and future unmanned-system infrastructures, that distinction marks the boundary between convenient experimentation and defensible performance evaluation.

From this same perspective, *AtlasRAN* suggests that the next generation of AI-RAN and open 5G evaluation environments should collapse the traditional boundary between “platform engineering” and “experimental method.” Rather than treating transport, synchronization, and observability as secondary implementation details, future architectures should expose timing discipline, bidirectional coupling semantics, and process-to-memory transfer behavior as first-class experimental variables, consistent with Twi-Net’s emphasis on measurable cyber-physical coupling and AutoRAN’s emphasis on engineered transport and clock discipline [5], [6]. This, in turn, motivates a tighter follow-on line of work in which host-OS best-effort assumptions are replaced by explicit timing contracts, engineered I/O paths, and fronthaul-aware synchronization, then re-evaluated under the same CU–DU multi-UE ablations to determine whether scaling recovers once decoder acceleration is no longer the dominant bottleneck. In particular, emerging AI-RAN simulation substrates, including NVIDIA’s Sionna-RT-inspired CUDA channel modeler, should be designed not only for protocol and channel realism, but also for controllable latency, measurable tail behavior, and explicit end-to-end coupling across compute, memory, and transport. For ubiquitous wireless infrastructure, this is the essential future direction: timing and I/O must be treated as first-class design requirements, because only then can p95/p99/p99.999 latency claims, concurrency limits, and shared-edge capacity conclusions be defended as trustworthy systems evidence rather than artifacts of a convenient harness.

VII. CONCLUSION

The O-RAN and AI-RAN ecosystem is heterogeneous not only in protocol coverage, but in *execution regime*: which components run where (CPU/GPU/NIC/accelerator), what interfaces are exposed, and whether the surrounding I/O and time-

scale assumptions are engineered or merely convenient. This paper reframed open 5G experimentation through the lens of ubiquitous wireless infrastructure for vehicular and future unmanned-system settings. Rather than treating platform choice as a secondary implementation detail, *AtlasRAN* showed that it is a first-order modeling and performance-evaluation decision. The paper contributed two anchor reference architectures, a terminology for separating functional compatibility from timing fidelity, and a capability matrix that maps common O-RAN and AI-RAN research questions to appropriate evaluation environments.

The CU-DU case study then made this point quantitative. On a coherent CPU-GPU edge platform, GPU offload substantially reduced decoder work, but multi-user uplink goodput still declined sharply under host-OS emulation as the number of users increased. Because fairness remained near ideal while CPU and GPU utilization decreased with load, the dominant limiter was not decoder saturation. It was the surrounding execution harness, whose online I/O and timing behavior under-fed the pipeline. This is the central systems result of the paper: once an important compute bottleneck is reduced, memory movement, transport semantics, and time coupling can become the real determinants of observed scalability. This complements broader edge-compute evidence that coherent memory and accelerator offload can create useful CPU headroom, while showing that the next bottleneck may sit in the surrounding execution harness.

For researchers studying 5G as a common infrastructure for road vehicles and future unmanned-system services, the practical implication is straightforward. Claims about scalability, real-time behavior, or shared edge capacity should only be made in environments whose timing and I/O properties are visible and appropriate to the claim. Future work should therefore move beyond protocol compatibility alone and toward evaluation pipelines that expose coupling semantics, synchronization discipline, and fronthaul-facing transport behavior as measurable variables.

REFERENCES

- [1] H. Bagheri *et al.*, “5g nr-v2x: Toward connected and cooperative autonomous driving,” *IEEE Communications Standards Magazine*, vol. 5, no. 1, pp. 48–54, 2021.
- [2] L. Liu *et al.*, “Vehicular edge computing and networking: A survey,” *Mobile Networks and Applications*, vol. 26, pp. 1145–1168, 2021, published online: 25 July 2020.
- [3] F. Kalteneberger *et al.*, “Openairinterface: Democratizing innovation in the 5g era,” *Computer Networks*, vol. 176, p. 107284, 2020.
- [4] A. Lacava *et al.*, “ns-O-RAN: Simulating O-RAN 5G systems in ns-3,” in *Proceedings of the 2023 Workshop on ns-3 (WNS3)*. Arlington, VA, USA: Association for Computing Machinery, 2023, pp. 35–44.
- [5] C. P. Robinson *et al.*, “Twinet: Connecting real world networks to their digital twins through a live bidirectional link,” in *Proceedings of the IEEE Global Communications Conference (GLOBECOM)*, Cape Town, South Africa, Dec. 2024.
- [6] S. Maxenti *et al.*, “Autoran: Automated and zero-touch open ran systems,” *arXiv preprint arXiv:2504.11233*, 2025. [Online]. Available: <https://arxiv.org/abs/2504.11233>
- [7] R. Barker *et al.*, “Six times to spare: Characterizing gpu-accelerated 5g ldpc decoding for edge-rsu communications,” 2026. [Online]. Available: <https://arxiv.org/abs/2602.04652>
- [8] M. Polese *et al.*, “Colosseum: The open ran digital twin,” *IEEE Open Journal of the Communications Society*, vol. 5, pp. 5452–5466, 2024.
- [9] D. Villa *et al.*, “X5g: An open, programmable, multi-vendor, end-to-end, private 5g o-ran testbed with nvidia arc and openairinterface,” *IEEE Transactions on Mobile Computing*, vol. 24, no. 11, pp. 11 305–11 322, 2025. [Online]. Available: <https://doi.org/10.1109/TMC.2025.3580764>
- [10] Open AI Cellular Project, “Open AI Cellular (OAI): An Open-Source Platform for Prototyping AI-Enabled O-RAN Control,” 2023, accessed: 2026-03-13. [Online]. Available: <https://www.openai-cellular.org/>
- [11] 6G-SANDBOX Consortium, “6G-SANDBOX: A pan-european testbed for 5g-advanced and 6g experimentation,” 2023, accessed: 2026-03-13. [Online]. Available: <https://6g-sandbox.eu/>
- [12] J. Hoydis *et al.*, “Sionna: An open-source library for next-generation physical layer research,” *arXiv preprint arXiv:2203.11854*, 2022. [Online]. Available: <https://arxiv.org/abs/2203.11854>
- [13] —, “Sionna RT: Differentiable ray tracing for radio propagation modeling,” *arXiv preprint arXiv:2303.11103*, 2023. [Online]. Available: <https://arxiv.org/abs/2303.11103>
- [14] S. Cammerer *et al.*, “Sionna research kit,” 2025, accessed: 2026-03-13. [Online]. Available: <https://nvlabs.github.io/sionna/rk/index.html>
- [15] J. Bocuzzi *et al.*, “GPU accelerated high capacity, AI-ready 5G/6G reference design and verification methodology,” *IEEE Wireless Communications*, vol. 32, no. 6, pp. 216–223, 2025.
- [16] K. Cohen-Arazi *et al.*, “NVIDIA AI aerial: AI-native wireless communications,” *arXiv preprint arXiv:2510.01533*, 2025. [Online]. Available: <https://arxiv.org/abs/2510.01533>
- [17] A. Ebrahimi and F. Afghah, “Intelligent task offloading: Advanced mec task offloading and resource management in 5g networks,” in *2025 IEEE Wireless Communications and Networking Conference (WCNC)*. Milan, Italy: IEEE, 2025, pp. 1–6.
- [18] AI-RAN Alliance, “Working groups / committees,” 2026, accessed: 2026-03-13. [Online]. Available: <https://ai-ran.org/working-groups/>
- [19] —, “Industry leaders in ai and wireless form ai-ran alliance,” 2024, accessed: 2026-03-13. [Online]. Available: <https://ai-ran.org/press-releases/alliance-formation>
- [20] M. Seidel *et al.*, “How to get away with OpenAirInterface: A practical guide to 5G RAN configuration,” in *2023 3rd International Conference on Electrical, Computer, Communications and Mechatronics Engineering (ICECCME)*, Tenerife, Spain, 2023.
- [21] srsRAN Project, “Configuration Reference — srsRAN Project Documentation,” 2025, accessed: 2026-03-13. [Online]. Available: https://docs.srsran.com/projects/project/en/latest/user_manuals/source/config_ref.html
- [22] P. Hintjens, *ZeroMQ: Messaging for Many Applications*. O’Reilly Media, Inc., 2013. [Online]. Available: <https://zeromq.org/>
- [23] OpenAirInterface Software Alliance, “Rf simulator (rfsim),” 2026, accessed: 2026-03-13. [Online]. Available: <https://github.com/OPENAIRINTERFACE/openairinterface5g/blob/develop/radio/rfsimulator/README.md>
- [24] srsRAN Project, “srsran gnb with srsue,” 2026, accessed: 2026-03-13. [Online]. Available: <https://docs.srsran.com/projects/project/en/latest/tutorials/source/srsUE/source/index.html>
- [25] —, “srsran gnb with amarisoft ue,” 2026, accessed: 2026-03-13. [Online]. Available: <https://docs.srsran.com/projects/project/en/latest/tutorials/source/amariUE/source/index.html>
- [26] —, “O-ran cu-du split,” 2026, accessed: 2026-03-13. [Online]. Available: https://docs.srsran.com/projects/project/en/latest/tutorials/source/cu_du_split/source/index.html
- [27] R. Schmidt and F. Kalteneberger, “Oai working practices, development process, and roadmap,” 2023, openAirInterface Software Alliance workshop slides. [Online]. Available: <https://openairinterface.org/wp-content/uploads/2023/11/Robert-Schmidt-Florian-Kalteneberger-OAIEURECOM.pdf>
- [28] srsRAN Project, “O-ran 7.2 ru guide,” 2026, accessed: 2026-03-13. [Online]. Available: <https://docs.srsran.com/projects/project/en/latest/tutorials/source/oranRU/source/index.html>
- [29] OpenAirInterface Software Alliance, “O-ran 7.2 fronthaul tutorial,” 2024, accessed: 2026-03-13. [Online]. Available: https://gitlab.eurecom.fr/oai/openairinterface5g/-/blob/v2.1.0/doc/ORAN_FH17.2_Tutorial.md
- [30] NVIDIA Corporation, *Aerial Omniverse Digital Twin 1.4.1 Documentation*, NVIDIA Corporation, 2026, accessed: 2026-03-13. [Online]. Available: <https://docs.nvidia.com/aerial/aerial-dt/index.html>
- [31] A. Lacava *et al.*, “Programmable and customized intelligence for traffic steering in 5g networks using open ran architectures,” *IEEE Transactions on Mobile Computing*, vol. 23, no. 4, pp. 2882–2897, 2024.
- [32] L. Mamushiane *et al.*, “Deploying a stable 5G SA testbed using srsRAN and open5gs: UE integration and troubleshooting towards network slicing,” in *2023 icABCD*, 2023.

- [33] OpenAirInterface Software Alliance, “5g sa tutorial with oai cn5g, oai gnb and cots ue,” 2026, accessed: 2026-03-13. [Online]. Available: https://gitlab.eurecom.fr/oai/openairinterface5g/-/blob/develop/doc/NR_SA_Tutorial_COTS_UE.md
- [34] E. Moro *et al.*, “An open ran framework for the dynamic control of 5g service level agreements,” in *2023 IEEE Conference on Network Function Virtualization and Software Defined Networks (NFV-SDN)*, 2023, pp. 141–146.
- [35] srsRAN Project, “srsran project documentation,” 2026, accessed: 2026-03-13. [Online]. Available: <https://docs.srsran.com/projects/project>
- [36] R. P. Alves *et al.*, “Experimental comparison of 5g sdr platforms: srsran x openairinterface,” *arXiv preprint arXiv:2406.01485*, 2024. [Online]. Available: <https://arxiv.org/abs/2406.01485>
- [37] A. Tripathi *et al.*, “Benchmarking software defined radio based 5G deployments with srsRAN: Lessons learned,” in *2025 IEEE Wireless Communications and Networking Conference (WCNC)*, 2025, pp. 1–6.
- [38] D. B. de Oliveira, D. Casini, and T. Cucinotta, “Operating system noise in the linux kernel,” *IEEE Transactions on Computers*, vol. 72, no. 1, pp. 196–207, 2023.
- [39] Intel Network and Edge Group, “Fec acceleration and DFT/iDFT (fft/iff) offloading with intel® vran boost,” Intel Corporation, Technical Report 786771, Aug. 2023, dated: 2023-08-22. [Online]. Available: <https://www.intel.com/content/www/us/en/content-details/786771/fec-acceleration-and-dft-idft-fft-iff-offloading-with-intel-vran-boost.html>
- [40] A. Butcher and J. Boccuzzi, “Exploring computing platforms for radio access networks: Heterogeneous computing at the network edge,” Dell EMC and Intel Corporation, White Paper, 2019, accessed: 2026-03-13. [Online]. Available: https://dl.dell.com/manuals/common/whitepaper_-_exploring_computing_platforms_for_radio_access_networks_v2.pdf
- [41] L. Lo Schiavo *et al.*, “CloudRIC: Open radio access network (O-RAN) virtualization with shared heterogeneous computing,” in *Proceedings of the 30th Annual International Conference on Mobile Computing and Networking (ACM MobiCom '24)*. Washington, DC, USA: Association for Computing Machinery, 2024, pp. 558–572.
- [42] A. Kelkar and C. Dick, “NVIDIA aerial GPU hosted AI-on-5G,” in *2021 IEEE 4th 5G World Forum (5GWF)*, Montreal, QC, Canada, 2021, pp. 64–69.
- [43] —, “A GPU hyperconverged platform for 5G vRAN and multi-access edge computing,” in *2021 IEEE Canadian Conference on Electrical and Computer Engineering (CCECE)*, Virtual / Ontario, Canada, 2021, pp. 1–6.
- [44] NVIDIA Corporation, “NVIDIA Aerial cuda-accelerated ran,” 2025, accessed: 2026-03-13. [Online]. Available: <https://github.com/NVIDIA/aerial-cuda-accelerated-ran>
- [45] R. Barker *et al.*, “Real: Reinforcement learning-enabled xapps for experimental closed-loop optimization in o-ran with osc ric and srsran,” in *2025 IEEE International Conference on Communications Workshops (ICC Workshops)*, 2025, pp. 389–395.
- [46] R. Kokku *et al.*, “Nvs: A substrate for virtualizing wireless resources in cellular networks,” *IEEE/ACM Transactions on Networking*, vol. 20, no. 5, pp. 1333–1346, 2012.
- [47] H. Cheng *et al.*, “Oranslice: An open-source 5g network slicing platform for o-ran,” in *Proceedings of the 30th Annual International Conference on Mobile Computing and Networking (ACM MobiCom '24)*. Association for Computing Machinery, 2024. [Online]. Available: <https://doi.org/10.1145/3636534.3701544>
- [48] POWDER, “Powder overview,” 2026, accessed: 2026-03-13. [Online]. Available: <https://docs.powderwireless.net/powder-overview.html>
- [49] A. E. Dorcheh, T. Seyfi, and F. Afghah, “DORA: Dynamic O-RAN resource allocation for multi-slice 5G networks,” *arXiv preprint arXiv:2509.07242*, 2025. [Online]. Available: <https://arxiv.org/abs/2509.07242>
- [50] Open Traffic Generator contributors, “Ixia-c traffic generator,” Open Traffic Generator, 2026, version v1.45.0-5; Accessed: 2026-03-13. [Online]. Available: <https://github.com/open-traffic-generator/ixia-c>